Electronic Supplementary Information

Synthesis of S-doped AuPbPt alloy Nanowire-networks as Superior Catalysts towards ORR and HER

Xiang Zhang,[a] Shibin Wang,[b] Chenshuo Wu,[a] Hong Li,[a] Yi Cao,[a] Shenggang Li,[c] and Haibing Xia[a,]*

[a]State Key Laboratory of Crystal Materials, Shandong University, Jinan, 250100, P. R. China;

[b] Institute of Industrial Catalysis, State Key Laboratory Breeding Base of Green-Chemical Synthesis Technology, College of Chemical Engineering, Zhejiang University of Technology, Hangzhou 310032, P.R. China.;

[c]CAS Key Laboratory of Low-Carbon Conversion Science and Engineering, Shanghai Advanced Research Institute, Chinese Academy of Sciences, 100 Haike Road, Shanghai 201210, China.

Corresponding Author:* (H. X.) E-mail: hbxia@sdu.edu.cn

Fig. S1 TEM images (a to d) of loose network-like ensembles of 2 nm Au NCs doped by Pb^{2+} ions (a), S-doped AuPb NWNs obtained by the one-time $NaBH_4$ reduction (b), $NaBH_4$ reduction for two times (c), $NaBH_4$ reduction for three times (d) and HAADF–STEM–EDS spectrum (e) of S-doped AuPb NWNs (c). The concentrations of Pb^{2+} ions used for synthesis of AuPb products and S-doped AuPb NWNs were 1.8 mM. The concentration of $NaBH_4$ is 0.1 mol L^{-1}.

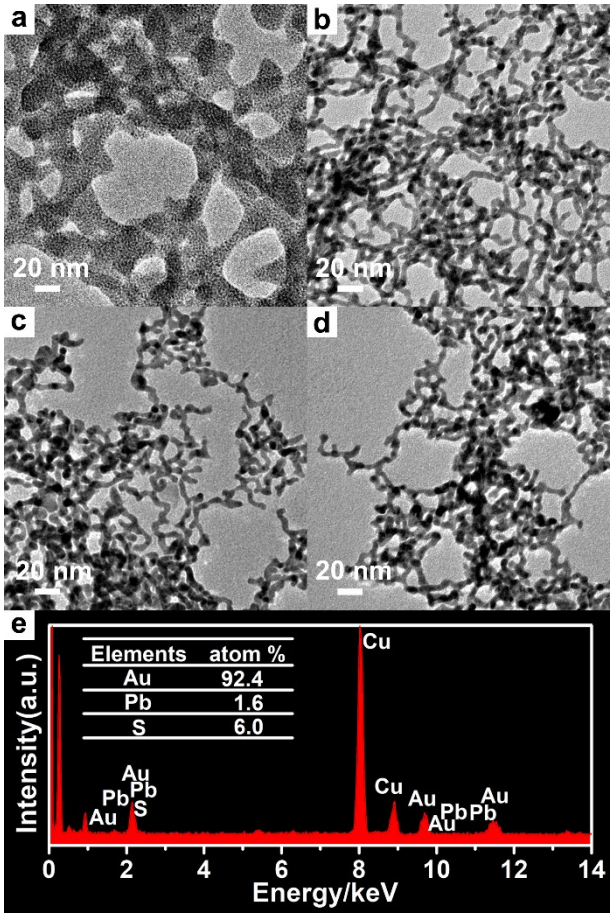

Initially, the average size of the ligaments of loosely network-like ensembles of 2 nm Au NCs doped by Pb^{2+} ions is 15.4 ± 6.2 nm (Fig. S1a), which can become smaller after the treatment of $NaBH_4$ reduction. In addition, the average size of the ligaments of the S-doped AuPb NWs obtained by the one-time $NaBH_4$ reduction, $NaBH_4$ reduction for two times and $NaBH_4$ reduction for three times are 5.5 ± 1.9 nm, 5.2 ± 1.6 nm and 5.0 ± 1.4 nm, respectively (Fig. S1b, S1c and S1d). Note that the amounts of Pb and S in the S-doped AuPb NWNs also change accordingly (refer to the later part).

Fig. S2 CV curve of S-doped AuPbPt alloy NWNs in N_2-saturated 0.1 M $HClO_4$ solution with a scan rate of 100 mV s^{-1}.

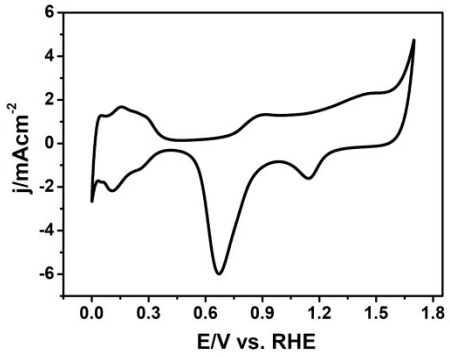

As shown in Fig. S2, S-doped AuPbPt alloy NWNs exhibit the obvious characteristic peaks of Pt (at about 0.67 V vs. RHE) and Au (at about 1.15 V vs. RHE) in acidic media, which indicates that the surfaces of S-doped AuPbPt alloy NWNs are composed of elemental Pt and Au.

Fig. S3 Energy dispersive X-ray spectroscopy (EDS) spectrum (A) of S-doped AuPbPt alloy NWNs and HAADF-STEM-EDS cross-sectional compositional line profile (B) of an individual S-doped AuPbPt alloy NW. The inset is HAADF-STEM image.

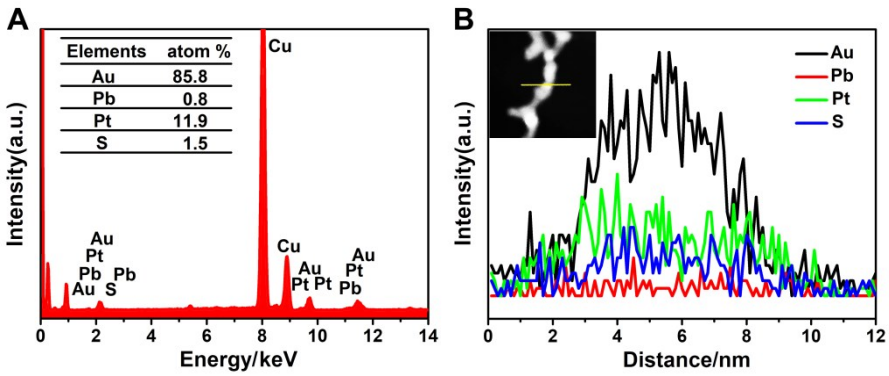

Fig. S4 XRD patterns of S-doped AuPb NWNs (black curve) and S-doped AuPbPt alloy NWNs (red curve), normalized for better comparison.

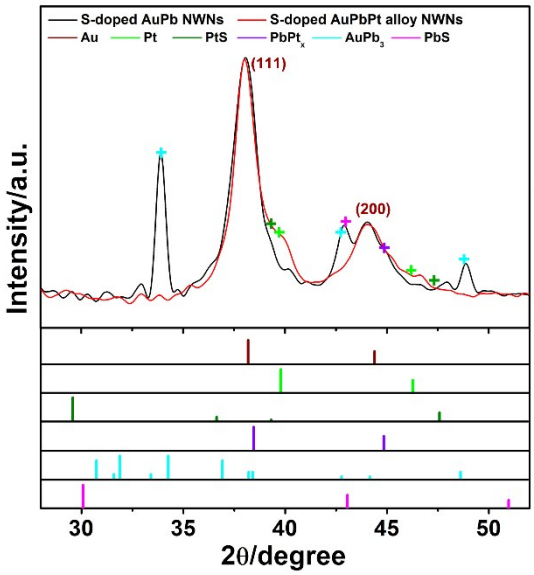

XRD patterns of S-doped AuPb NWNs (black curve) and S-doped AuPbPt alloy NWNs (red curve) was normalized according to the intensity of Au(111) diffraction peak for better comparison. Since the intensity of diffraction peak of $AuPb_3$ at 42.8° is rather lower than that of $AuPb_3$ at 48.9° in the JCPDS card no.26-0711. Accordingly, the intensity of diffraction peak of $AuPb_3$ at 42.8° should be lower than that of $AuPb_3$ at 48.9° in the S-doped AuPbPt alloy NWNs (red curve). Therefore, the contribution of diffraction peak of $AuPb_3$ at 42.8° in the diffraction peak at between 41.7° to 48.2° (black curve) should be minor and the diffraction peak at 42.9° (magenta crosses) can be assigned to PbS (JCPDS card no.05-0592), instead of $AuPb_3$ at 42.8°. Moreover, the shoulder peak at 38.7° in the XRD pattern of the S-doped AuPbPt alloy NWNs can be assigned to Pt (green crosses) and/or PtS (olive crosses). Furthermore, the slight broadening on the right of the diffraction peak at between 41.7° to 48.2° (red curve) indicates the formation of $PbPt_x$ (violet crosses and JCPDS card no.06-0574).

Fig. S5 CO stripping voltammograms of commercial Pt/C catalysts (A) and S-doped AuPbPt alloy NWNs (B) in 0.5 M H_2SO_4 solution at a scan rate of 50 mV s^{-1}. The solid red line corresponds to the first cycle, while the second cycle is displayed as short dashed black line.

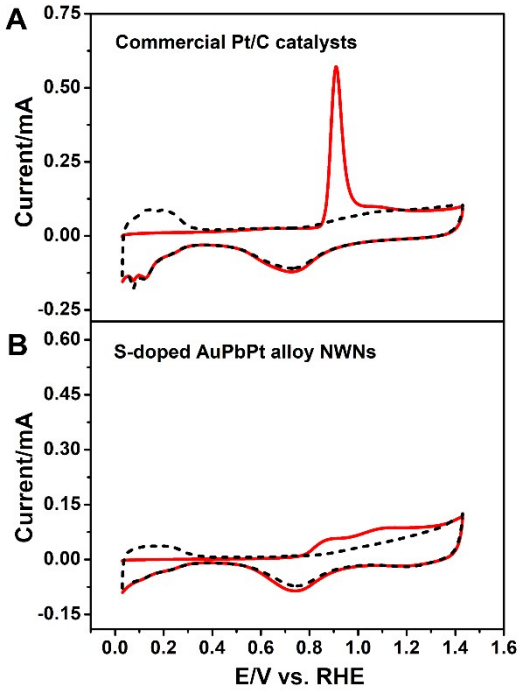

In their CO stripping voltammograms, commercial Pt/C catalysts exhibit a typically sharp CO-stripping peak while S-doped AuPbPt alloy NWNs exhibit a much broader one. This result indicates that the surfaces of the as-prepared S-doped AuPbPt alloy NWNs are not the continuous pure Pt-skin, but the Pt-based alloy skin.[1]

Moreover, the onset potential (0.78 V vs. RHE) of S-doped AuPbPt alloy NWNs is also more negative than that of commercial Pt/C catalysts (0.85 V vs. RHE), suggesting that S-doped AuPbPt alloy NWNs have a weak adsorption energy and better CO removal ability.[2,3] That is, S-doped AuPbPt alloy NWNs may have a better removal ability for oxygen-containing species or intermediates.

However, the potential range for CO adsorption of S-doped AuPbPt alloy NWNs is much broader than that of commercial Pt/C catalysts. Accordingly, the adsorption ability of the reactants (such as O_2) on S-doped AuPbPt alloy NWNs may be maintained because of the increasing adsorption potential range, which can make up the loss in their adsorption ability.[4]

Fig. S6 XPS spectra of S 2p (A) and O 1s (B) of S-doped AuPbPt alloy NWNs.

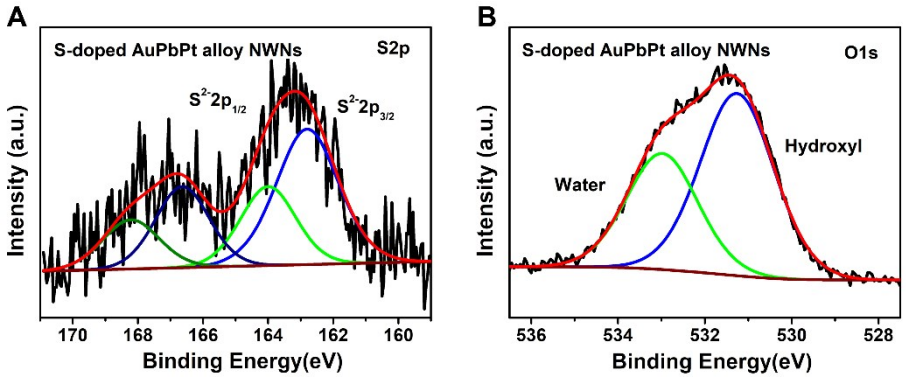

As shown in Fig. S6A, the main binding energy (BE) of S 2p signals of S-doped AuPbPt alloy NWNs are 162.8 eV and 164.1 eV, which correspond to the S $2p_{3/2}$ and S $2p_{1/2}$ of S^{2-} species,[5] respectively. In addition, BEs of O 1s signal located at about 531.3 eV and 533.0 eV could be ascribed to the surface hydroxyl groups and adsorbed water,[6] respectively, instead of the lattice oxygen.

Fig. S7 XPS spectra of Pt 4f (A) and Au 4f (B) of pure Pt NPs and Au NPs, respectively.

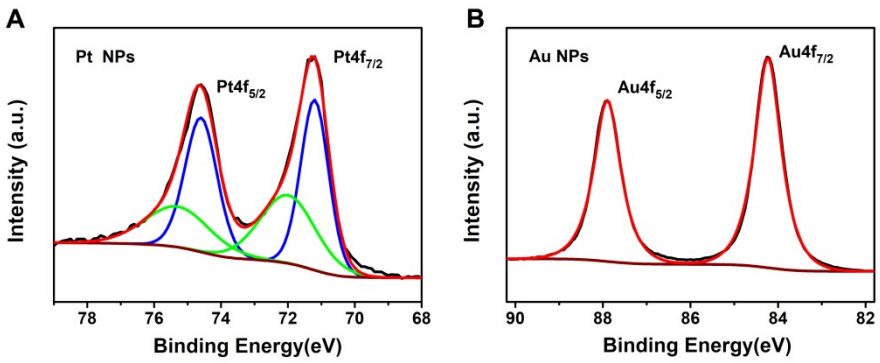

As shown in Fig. S7A, the binding energy (BE) of Pt 4f signals of Pt NPs are 71.2 eV and 74.6 eV, which assigned to the Pt $4f_{7/2}$ and Pt $4f_{5/2}$ of metallic Pt(0), respectively. Moreover, BEs of Pt signal located at about 72.0 eV and 75.4 eV could be ascribed to the Pt(II) species.

Fig. S7B shows that BEs of Au $4f_{7/2}$ and Au $4f_{5/2}$ of metallic Au(0) are located at 84.2 eV and 87.9 eV, respectively.

Fig. S8 TEM images of network-like AuPb products obtained at different concentrations of additional Pb^{2+} ions: 2.0 mM (a), 2.2 mM (b) and 2.4 mM (c). The particle number concentration of Au NCs is about 1.06×10^{15} /mL in the mixture solution. All of the reaction times are 1 h at room temperature.

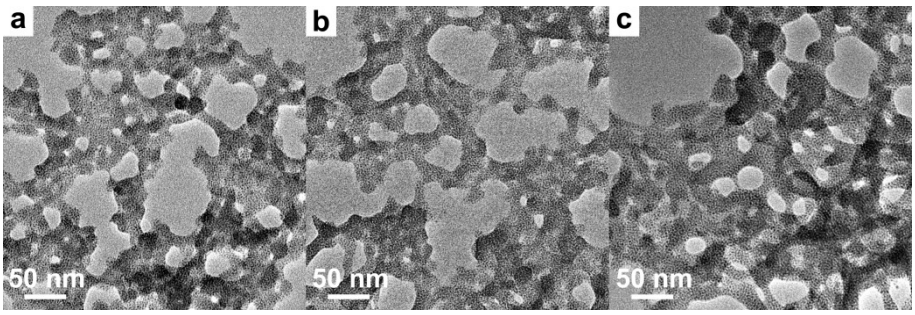

It can be observed that network-like AuPb products can be obtained when the concentration of additional Pb^{2+} ions is greater than 1.8 mM (Fig. S8). In addition, the obtained network-like AuPb products are rather similar in the morphology. Thus, the minimal concentration of Pb^{2+} ions used for synthesis of S-doped AuPb NWNs is 1.8 mM.

Fig. S9 TEM images of the Au-Pt products obtained without (A) and with (B) the addition of Pb^{2+} ions by AA reduction of Pt precursor in the solution containing 2 nm Au NCs. The concentration of Pb^{2+} ions (in sample B) is 1.8 mM. The corresponding concentration of Pt precursor for synthesis of the two types of Au-Pt products is 0.22 mM.

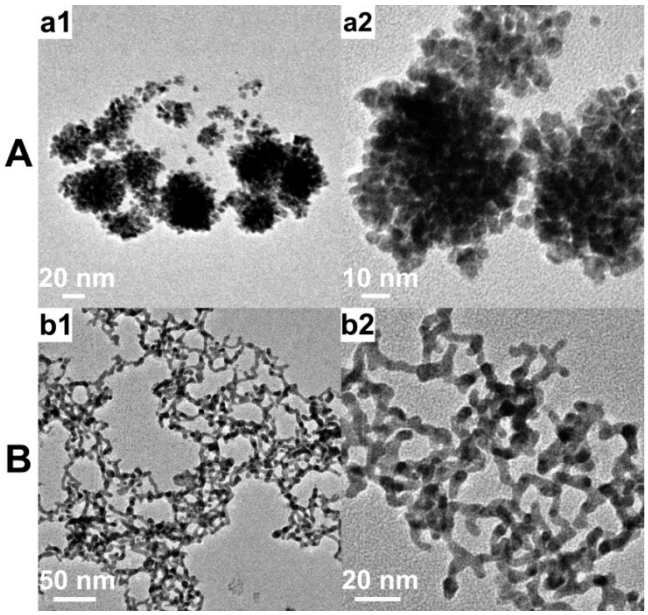

The role of addition Pb^{2+} ions is to assist the formation of network-like ensemble of Au NCs, instead of dispersed Au NCs. Accordingly, in the absence of Pb^{2+} ions, multi-branched Au-Pt products with an average diameter of 42.9 ± 12.0 nm were obtained (Fig. S9A), which were similar with those reported. However, in the presence of Pb^{2+} ions (> 1.8 mM), network-like Au-Pt products with an average diameter of 6.0 ± 1.3 nm were obtained (Fig. S9B) due to the formation of network-like AuPb templates.

Fig. S10 LSV curves (A) and histograms (B) of half-wave potentials ($E_{1/2}$) of four types of S-doped $AuPb_mPt$ alloy NWNs (a to d) prepared by using the corresponding four types of S-doped $AuPb_m$ NWNs as templates, m represents the concentration of Pb^{2+} ions used for synthesis of four types of S-doped AuPb NWNs. These LSV curves were measured at 1600 rpm in O_2-saturated 0.1 M $HClO_4$. The concentrations of Pb^{2+} ions (m) used for synthesis of four types of S-doped AuPb NWNs were 1.8 mM (a), 2.0 mM (b), 2.2 mM (c) and 2.4 mM (d), respectively. The concentration of Pt precursor for synthesis of four types of S-doped $AuPb_mPt$ alloy NWNs is 0.22 mM.

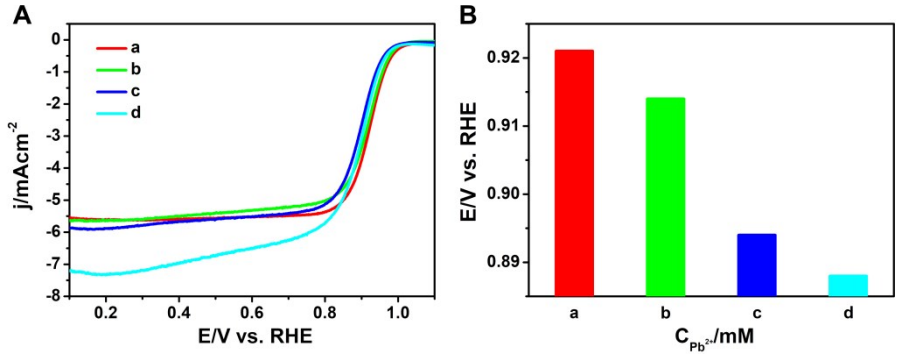

The formation of network-like AuPb templates is essential for the synthesis of AuPt NWNs. However, the presence of elemental Pb in the final AuPbPt NWNs also can impact their electrocatalytic performance. Thus, four types of network-like AuPb templates were prepared and then used for synthesis of the corresponding AuPt NWNs. The electrocatalytic performances of four types of AuPt NWNs towards to ORR were evaluated by LSV curves and the corresponding $E_{1/2}$ (Fig. S10).

The $E_{1/2}$ of S-doped $AuPb_{1.8}Pt$ alloy NWNs, S-doped $AuPb_{2.0}Pt$ alloy NWNs, S-doped $AuPb_{2.2}Pt$ alloy NWNs and S-doped $AuPb_{2.4}Pt$ alloy NWNs were 0.921, 0.914, 0.894 and 0.888 V, respectively. This result indicated that the ORR activity of S-doped AuPbPt alloy NWNs was decreased with the increase of the concentration of Pb^{2+} ions and S-doped $AuPb_{1.8}Pt$ alloy NWNs may have the best electrocatalytic activity towards ORR.

In our case, the minimal concentration of Pb^{2+} ions used for synthesis of S-doped AuPb NWNs was 1.8 mM. In fact, the content of Pb in the initial S-doped $AuPb_{1.8}$ NWNs is still higher, which have to be treated by $NaBH_4$ reduction for two times for the removal of extra Pb.

Fig. S11 LSV curves (A) and histograms (B) of half-wave potentials ($E_{1/2}$) of three types of S-doped AuPbPt alloy NWNs obtained by using the corresponding S-doped AuPb NWNs which were obtained by the one-time $NaBH_4$ reduction (a, black curve), $NaBH_4$ reduction for two times (b, red curve) and $NaBH_4$ reduction for three times (c, green curve). These LSV curves were measured at 1600 rpm in O_2-saturated 0.1 M $HClO_4$. The concentration of $NaBH_4$ is 0.1 mol L^{-1}. The concentrations of Pb^{2+} ions used for synthesis of S-doped AuPb NWNs were 1.8 mM. The concentration of Pt precursor for synthesis of S-doped AuPbPt alloy NWNs is 0.22 mM.

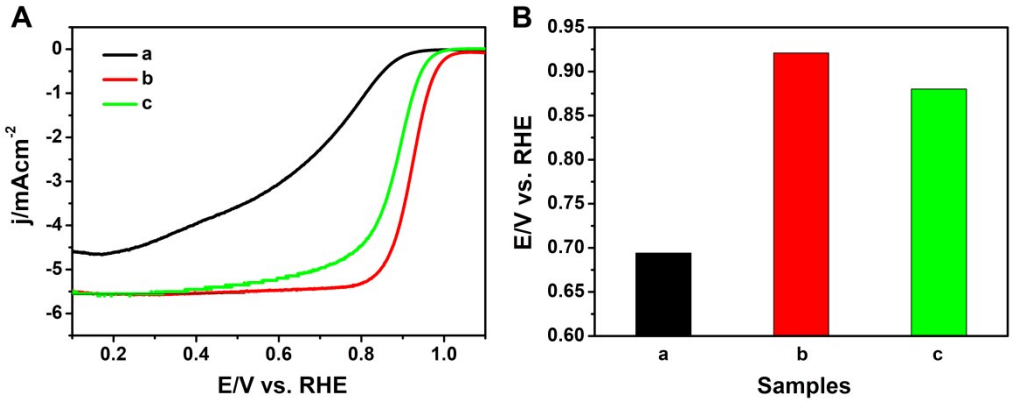

The presence of a proper amount of elemental S in the final AuPt NWNs can improve their electrocatalytic performance. Thus, three types of network-like AuPb templates were further prepared and then used for synthesis of the corresponding AuPbPt NWNs. The electrocatalytic performances of three types of S-doped AuPbPt alloy NWNs towards to ORR were evaluated by LSV curves and the corresponding $E_{1/2}$ (Fig. S11).

The $E_{1/2}$ of three types of S-doped AuPbPt alloy NWNs prepared by the one-time $NaBH_4$ reduction, $NaBH_4$ reduction for two times and $NaBH_4$ reduction for three times were 0.694, 0.921 and 0.880 V, respectively. This result indicated that S-doped $AuPb_{1.8}Pt$ alloy NWNs obtained by $NaBH_4$ reduction for two times may have the best electrocatalytic activity towards ORR. In addition, the amount of elemental S as well as Pb in the final AuPt NWNs can become proper after $NaBH_4$ reduction for two times.

Fig. S12 TEM images of AuPbPt products obtained under different pH values: 7.0 (a), 2.4 (b), 2.1 (c), and 2.0 (d). The concentration of Pt precursor for synthesis of AuPbPt products is 0.22 mM. The concentration of Pb^{2+} ions used for synthesis of S-doped AuPb NWNs is 1.8 mM. The proper amount of Pb and S in the S-doped AuPb NWNs was achieved by $NaBH_4$ reduction for two times.

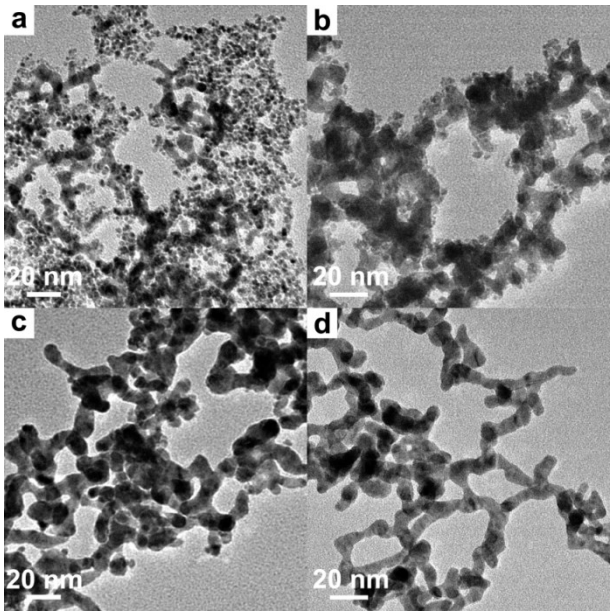

When the pH value of the reaction solution was 7.0, plenty of small Pt clusters as byproducts were formed, instead of conformal growth onto the surfaces of S-doped AuPb NWNs (Fig. S12a). When the pH value of the reaction solution was adjusted from 7.0 to 2.4 and 2.1, the amount of small Pt clusters gradually become fewer (Fig. S12b and c). When the pH value of the reaction solution was as low as 2.0, there is hardly any small Pt cluster observed (Fig. S12d), indicating the successful conformal growth of Pt onto S-doped AuPb NWNs.

Fig. S13 TEM images of S-doped AuPbPt NWNs obtained by using S-doped AuPb NWNs with a proper amount of Pb and S as templates and using different concentrations of Pt precursor: 0.11 mM (a), 0.22 mM (b), 0.24 mM (c), and 0.26 mM (d). The concentration of Pb^{2+} ions used for synthesis of S-doped AuPb NWNs is 1.8 mM. The S-doped AuPb NWNs with a proper amount of Pb and S was achieved by $NaBH_4$ reduction for two times. The pH value of the reaction media containing Pt precursor is about 2.

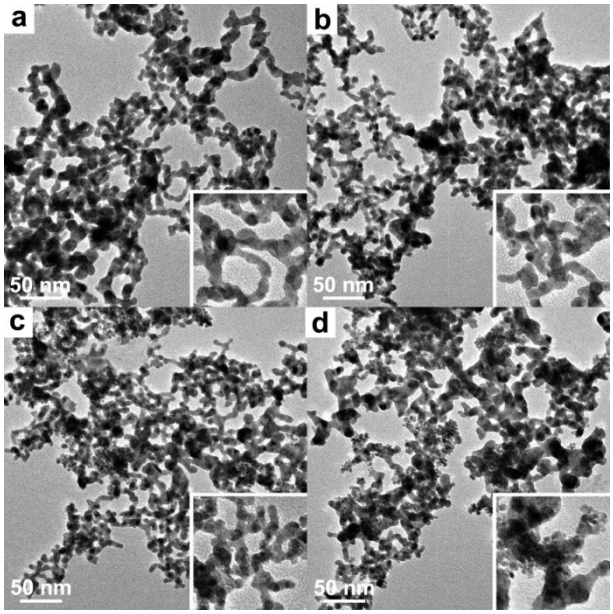

When the concentrations of Pt precursor were below 0.22 mM, the resulting S-doped AuPbPt alloy NWNs have a smooth surface and no any small Pt cluster was formed (Fig. S13a and S13b). However, with further increasing concentrations of Pt precursor, the amount of small Pt cluster gradually increased (Fig. S13c and S13d).

To determine the optimal concentration of Pt precursor, the electrocatalytic performance of these four types of S-doped AuPbPt NWNs towards to ORR and HER were evaluated by LSV curves and the corresponding $E_{1/2}$ and overpotential (Fig. S14 and S15).

Fig. S14 LSV curves (A) and histograms (B) of $E_{1/2}$ of S-doped $AuPbPt_m$ alloy NWNs obtained by using S-doped AuPb NWNs with a proper amount of Pb and S as templates and using different concentrations of Pt precursor: 0.11 mM (a), 0.22 mM (b), 0.24 mM (c), and 0.26 mM (d). The subscript number (m) represents the concentration of Pt precursor used for synthesis of S-doped $AuPbPt_m$ alloy NWNs. The concentration of Pb^{2+} ions used for synthesis of S-doped AuPb NWNs is 1.8 mM. S-doped AuPb NWNs with a proper amount of Pb and S was achieved by $NaBH_4$ reduction for two times. The pH value of the reaction media containing Pt precursor is about 2.

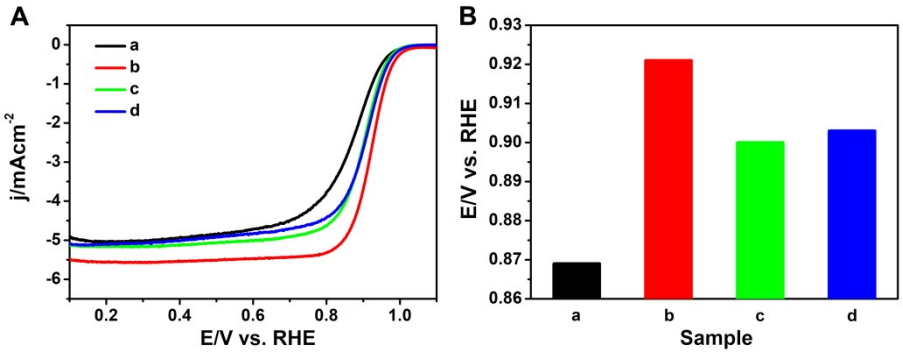

The $E_{1/2}$ of S-doped $AuPbPt_{0.11}$ alloy NWNs, S-doped $AuPbPt_{0.22}$ alloy NWNs, S-doped $AuPbPt_{0.24}$ alloy NWNs and S-doped $AuPbPt_{0.26}$ alloy NWNs were 0.869, 0.921, 0.900, and 0.903 V, respectively. This result indicated that S-doped $AuPbPt_{0.22}$ alloy NWNs may have the best electrocatalytic activity towards ORR.

Fig. S15 LSV curves (A), Tafel plots (B), histograms of mass activity (C) at -0.05 V (vs RHE) and current density (D) at -0.07V (vs RHE) of S-doped $AuPbPt_m$ alloy NWNs obtained by using S-doped AuPb NWNs with a proper amount of Pb and S as templates and using different concentrations of Pt precursor: 0.11 mM (a), 0.22 mM (b), 0.24 mM (c), and 0.26 mM (d). The subscript number (m) represents the concentration of Pt precursor used for synthesis of S-doped $AuPbPt_m$ alloy NWNs. The concentration of Pb^{2+} ions used for synthesis of S-doped AuPb NWNs is 1.8 mM. S-doped AuPb NWNs with a proper amount of Pb and S was achieved by $NaBH_4$ reduction for two times. The pH value of the reaction media containing Pt precursor is about 2.

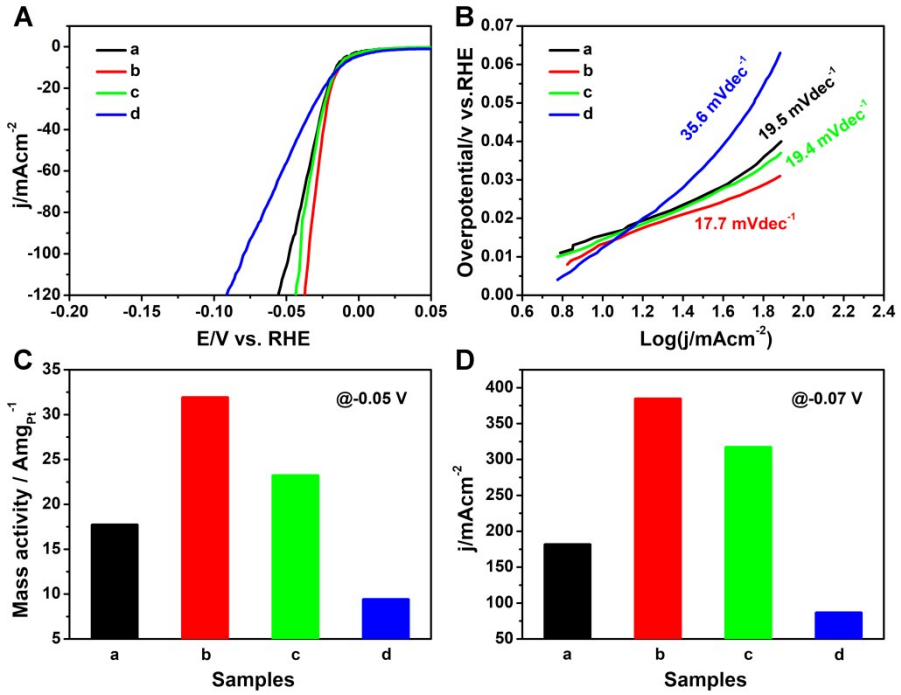

As shown in Fig. S15A, the overpotential at 10 mA cm^{-2} of S-doped $AuPbPt_{0.11}$ alloy NWNs, S-doped AuPb $Pt_{0.22}$ alloy NWNs, S-doped $AuPbPt_{0.24}$ alloy NWNs and S-doped $AuPbPt_{0.26}$ alloy NWNs were 16, 12, 15 and 14 mV, respectively. In addition, their corresponding Tafel plots were 19.5, 17.7, 19.4 and 35.6 mV dec^{-1}, respectively (Fig. S15B). Moreover, their mass activity (at -0.05V vs. RHE) were 17.7, 31.9, 23.2 and 9.4 A mg^{-1}, respectively (Fig. S15C). Furthermore, their current density (at -0.07 V vs. RHE) were 181.4, 387.4, 317 and 86.5 mA cm^{-2}, respectively (Fig. S15D). These results indicate that with the increasing concentrations of Pt precursor, their HER activity shows a volcano-type tendency. Moreover, S-doped $AuPbPt_{0.22}$ alloy NWNs exhibits the best HER activity, which also have the best ORR activity.

Fig. S16 CV curve of S-doped AuPb NWNs measured in N_2-saturated 0.1 M $HClO_4$ solution.

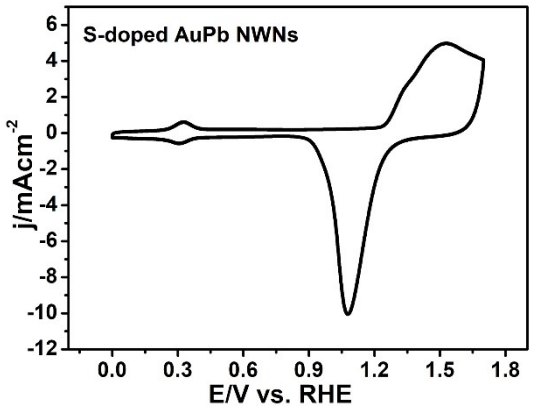

As shown in Fig. S16, the obvious peak at about 1.1 V vs. RHE is ascribed to the reduction peak of elemental Au, indicating that the surface of the as-prepared S-doped AuPb NWNs is mainly covered by elemental Au. In addition, a pair of peaks around 0.3 V vs. RHE are ascribed to oxidation and reduction peaks of Pb/PbS, indicating a small amount of Pb/PbS also exist on the surface of the as-prepared S-doped AuPb NWNs. The result is also in consistent with XRD results.

Fig. S17 CV curves of a series of S-doped AuPbPt alloy NWNs measured in N_2-saturated 0.1 M $HClO_4$ solution. These S-doped AuPbPt alloy NWNs were prepared by using different concentrations of Pt precursors (a to c) in the presence of the same S-doped AuPb NWNs as templates: 0.055 mM (a, black curve), 0.11 mM (b, red curve), 0.22 mM (c, green curve).

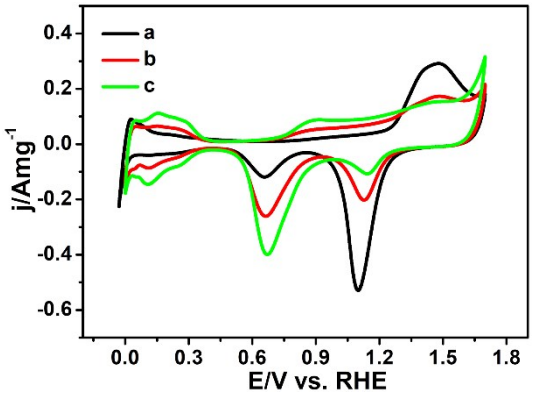

As mentioned above, the surface of the as-prepared S-doped AuPb NWNs is mainly covered by elemental Au (Fig. S16). However, when the concentration of Pt precursors used for synthesis of S-doped AuPbPt alloy NWNs increased from 0.055 to 0.11 and 0.22 mM, the reduction peaks of elemental Au around 1.1 V vs. RHE gradually becomes smaller. Meanwhile, the reduction peaks of elemental Pt around 0.66 V vs. RHE gradually become bigger. Accordingly, the hydrogen adsorption/desorption region between 0 and 0.4 V also become bigger. Note that the presence of the reduction peaks of elemental Au in the final S-doped AuPbPt alloy NWNs (Fig.R17c, the optimal sample in our case) indicates the presence of elemental Au on their surfaces and the final S-doped AuPb alloy NWNs are not fully covered by the formed Pt layer. These results indicate that additional Pt precursors are mainly reduced onto the surface of the of S-doped AuPb NWNs and the formed Pt layer is rather ultrathin. In comparison with S-doped AuPb alloy NWNs (Fig. R16), oxidation and reduction peaks of Pb/PbS (around 0.3 V vs. RHE) disappear in the S-doped AuPbPt alloy NWNs (Fig. S17). In addition, the main chemical state of element S in the XPS spectrum of S-doped AuPbPt alloy NWNs is S^{2-} (Fig.S6A). These results indicate that Pb/PbS in S-doped AuPb alloy NWNs indeed transforms into PtS and $PbPt_x$ in S-doped AuPbPt alloy NWNs, combined with XRD results mentioned above (Fig. 2). Since PbS mainly existed on the surfaces of S-doped AuPb NWNs, PtS and PbPtx should also mainly formed on the surfaces of S-doped AuPbPt alloy NWNs. Briefly, Pt, PtS and $PbPt_x$ all mainly exist on the surface of S-doped AuPbPt alloy NWNs.

Fig. S18 LSV curves of S-doped AuPbPt alloy NWNs in O_2-saturated 0.1 M $HClO_4$ solution at a scan rate of 10 mV s^{-1} over a range of rotation speed from 400 to 2025 rpm.

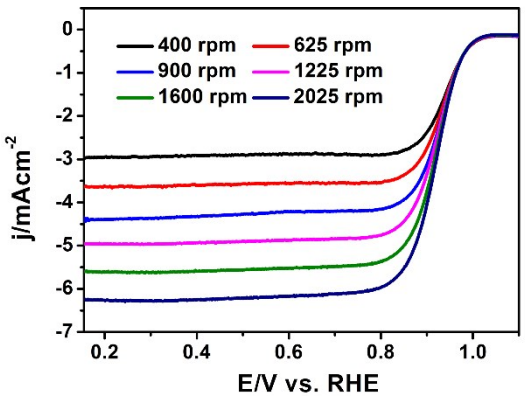

The number of electrons transferred (n) and kinetic current density (j_k) are obtained from the Koutecky-Levich equation:[7]

$$\frac{1}{j} = \frac{1}{j_k} + \frac{1}{j_d} = \frac{1}{j_k} + \frac{1}{B\omega^{1/2}}$$

$$B = 0.62nFC_0D_0^{2/3}\nu^{-1/6}$$

where j is the measured current density, j_k is the kinetic current density, and j_d is the diffusion limiting current density. ω is the angular velocity ($\omega = 2\pi N$, N is the linear rotation speed); n is the number of electrons transferred in the whole reaction; F is Faraday constant (96485 C mol^{-1}); C_0 is the bulk concentration of dissolved oxygen (1.18×10^{-6} mol cm^{-3} in 0.1 M $HClO_4$); D_0 is the diffusion coefficient of dissolved oxygen (1.93×10^{-5} cm^2 s^{-1} in 0.1 M $HClO_4$); ν is the kinematic viscosity (8.93×10^{-3} cm^2 s^{-1} for 0.1 M $HClO_4$).[8]

Fig. S19 LSV curves (A) of commercial Pt/C catalysts in O_2-saturated 0.1 M $HClO_4$ solution at a scan rate of 10 mV s^{-1} over a range of rotation speed from 400 to 2025 rpm. Koutecky-Levich (K-L) plots (B) of commercial Pt/C catalysts within the potential range from 0.2 to 0.5 V (vs RHE).

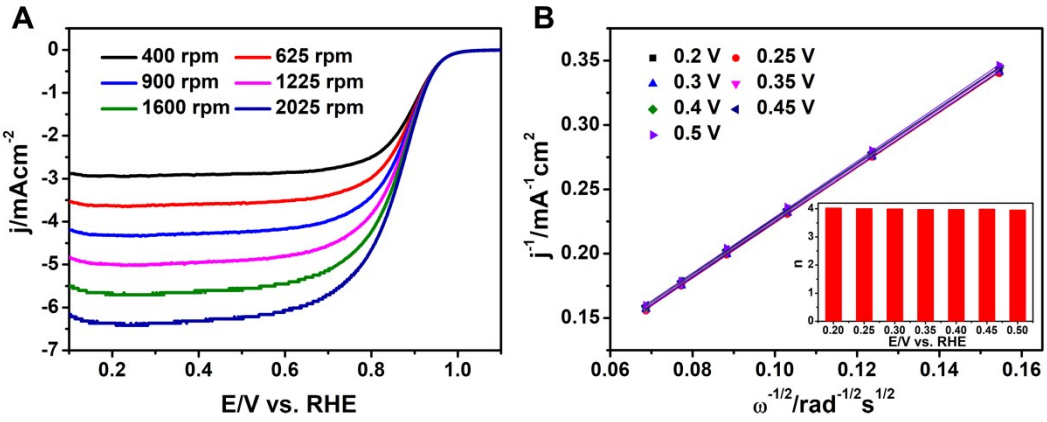

Fig. S20 Typical TEM images of steps defects (a and b) and deformation twinning (c-f) in the as-prepared S-doped AuPbPt alloy NWNs.

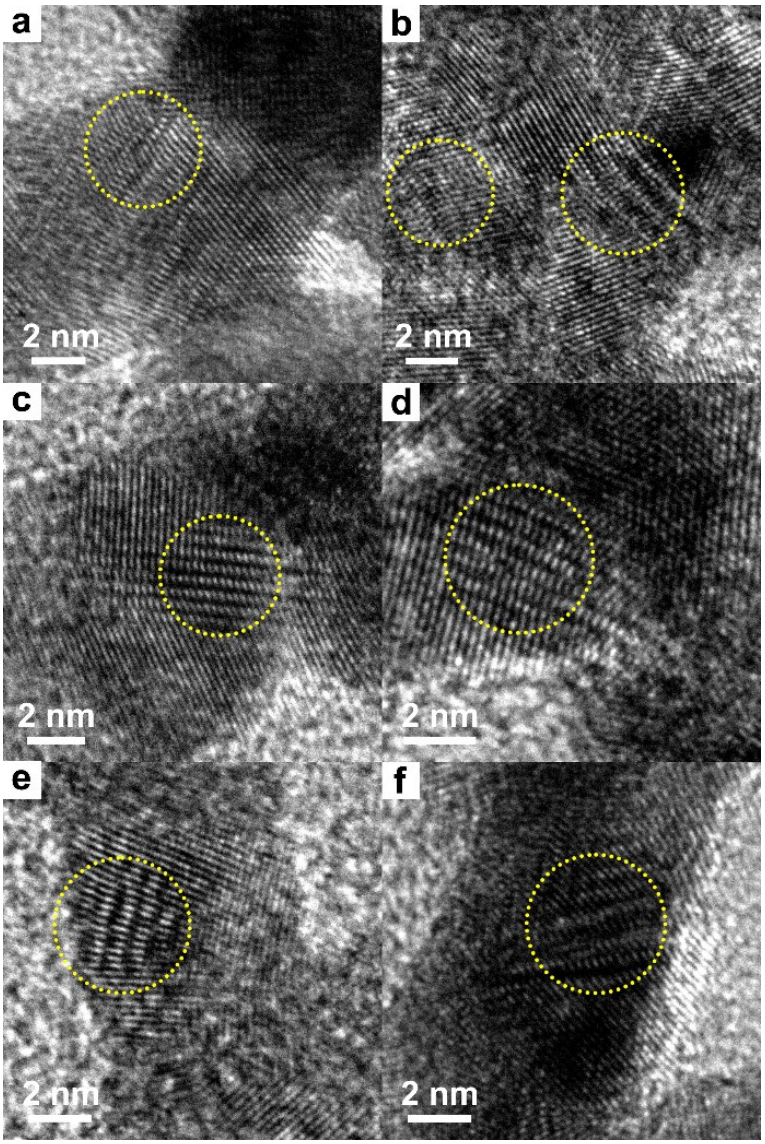

Fig. S21 LSV curves of commercial Pt/C catalysts before (black color) and after ADT between 0.6 and 1.1 V at scan rate of 100 mV s^{-1} in 0.1 M $HClO_4$ solution.

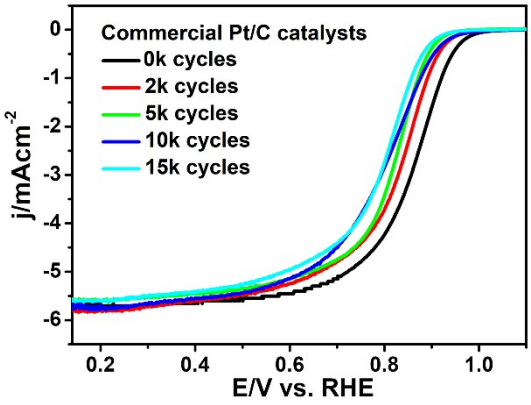

Fig. S22 LSV curves of S-doped AuPbPt alloy NWNs (solid curves) and commercial Pt/C catalysts (short dash curves) before (black color) and after ADT between 0.6 and 1.1 V at scan rate of 100 mV s^{-1} in 0.1 M $HClO_4$ solution.

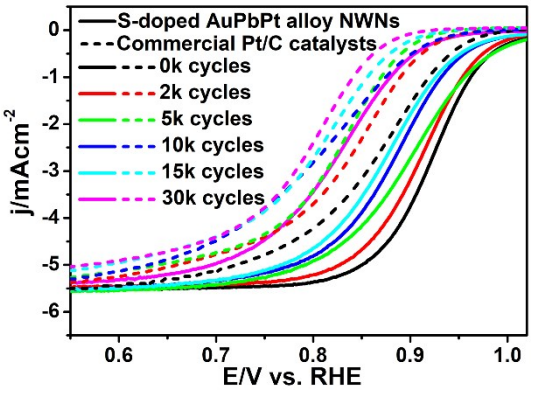

After ADT of 2k, 5k, 10k, 15k and 30k cycles, the $E_{1/2}$ values of the S-doped AuPbPt alloy NWNs decrease from the initial 0.921 V to 0.906, 0.903, 0.881, 0.874 and 0.822 V, respectively, while those of commercial Pt/C catalysts decrease from the initial 0.861 V to 0.830, 0.824, 0.802, 0.798 and 0.792 V, respectively (Fig. S22). One can see that the $E_{1/2}$ values of the S-doped AuPbPt alloy NWNs are higher than those commercial Pt/C catalysts obtained after ADT of the same cycles. The result illustrates that the durability of the present S-doped AuPbPt alloy NWNs is better than that of commercial Pt/C catalysts.

Fig. S23 Histograms of the original (A) and the normalized (B) current density at 0.7V vs RHE of S-doped AuPbPt alloy NWNs (solid histograms) and commercial Pt/C catalysts (sparse histograms) before (black color) and after ADT between 0.6 and 1.1 V at scan rate of 100 mV s^{-1} in 0.1 M $HClO_4$ solution.

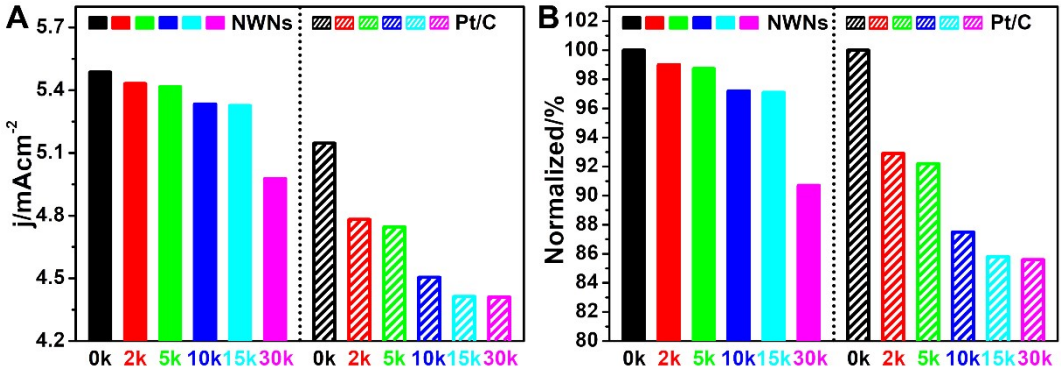

After ADT of 2k, 5k, 10k, 15k and 30k cycles, the current densities (at 0.7 V vs. RHE) of the S-doped AuPbPt alloy NWNs decrease from the initial 5.49 mA cm^{-2} to 5.43, 5.42, 5.33, 5.32 and 4.98 mA cm^{-2}, respectively, while those of commercial Pt/C catalysts decrease from the initial 5.15 mA cm^{-2} to 4.78, 4.75, 4.51, 4.42 and 4.41 mA cm^{-2}, respectively. One can see that the current densities (at 0.7 V vs. RHE) of the S-doped AuPbPt alloy NWNs are higher than those commercial Pt/C catalysts obtained after ADT of the same cycles. Moreover, the current density (at 0.7 V vs. RHE) of S-doped AuPbPt alloy NWNs after ADT of 2k, 5k, 10k, 15k and 30k cycles are 99.0, 98.7, 97.2, 97.1 and 90.7% of the initial current densities, respectively, while those of commercial Pt/C catalysts are 92.9, 92.2, 87.5, 85.8 and 85.6% of the initial current densities, respectively. Similarly, one can see that the percentage variation in the current densities (at 0.7 V vs. RHE) of the S-doped AuPbPt alloy NWNs are lower than those of commercial Pt/C catalysts obtained after ADT of the same cycles. These results illustrate that the durability of the present S-doped AuPbPt alloy NWNs is better than that of commercial Pt/C catalysts.

Fig. S24 Histograms of the original (A) and normalized (B) ECSA of S-doped AuPbPt alloy NWNs (solid histograms) and commercial Pt/C catalysts (sparse histograms) before (black color) and after ADT between 0.6 and 1.1 V at scan rate of 100 mV s^{-1} in 0.1 M $HClO_4$ solution.

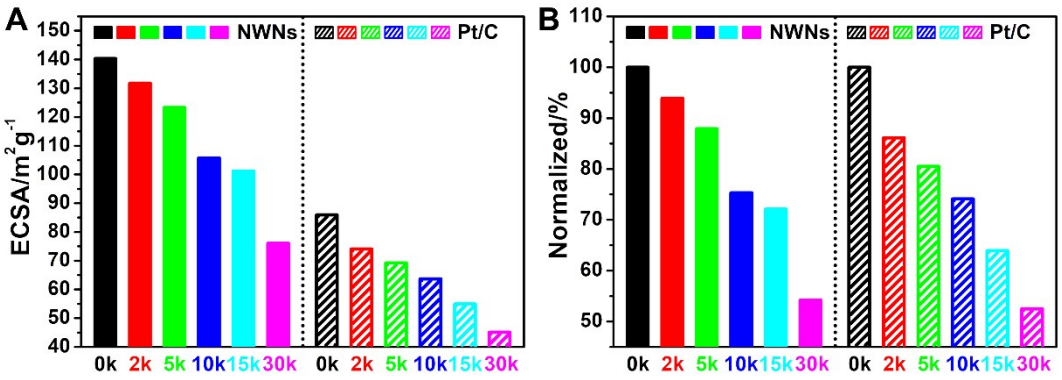

After ADT of 2k, 5k, 10k, 15k and 30k cycles, the ECSA values of S-doped AuPbPt alloy NWNs decrease from the initial 140.35 m^2 g^{-1} to 131.76, 123.31, 105.70, 101.21 and 76.06 m^2 g^{-1}, respectively, while those of commercial Pt/C catalysts decrease from the initial 85.96 m^2 g^{-1} to 74.05, 69.21, 63.67, 54.92 and 45.13 m^2 g^{-1}, respectively. One can see that ECSA values of the S-doped AuPbPt alloy NWNs are higher than those of commercial Pt/C catalysts obtained after ADT of the same cycles. Moreover, the ECSA values of S-doped AuPbPt alloy NWNs after ADT of 2k, 5k, 10k, 15k and 30k cycles are 93.9, 87.9, 75.3, 72.1 and 54.2% of the initial ECSA value, respectively, while those of commercial Pt/C catalysts are 86.1, 80.5, 74.1, 63.9 and 52.5% of the initial ECSA value, respectively. Similarly, one can see that the percentage variation in the ECSA value of the S-doped AuPbPt alloy NWNs are lower than those commercial Pt/C catalysts obtained after ADT of the same cycles. These results illustrate that the durability of the present S-doped AuPbPt alloy NWNs is better than that of commercial Pt/C catalysts.

Fig. S25 TEM images of S-doped AuPbPt alloy NWNs before (a) and after (b) the ADT of 2k cycles.

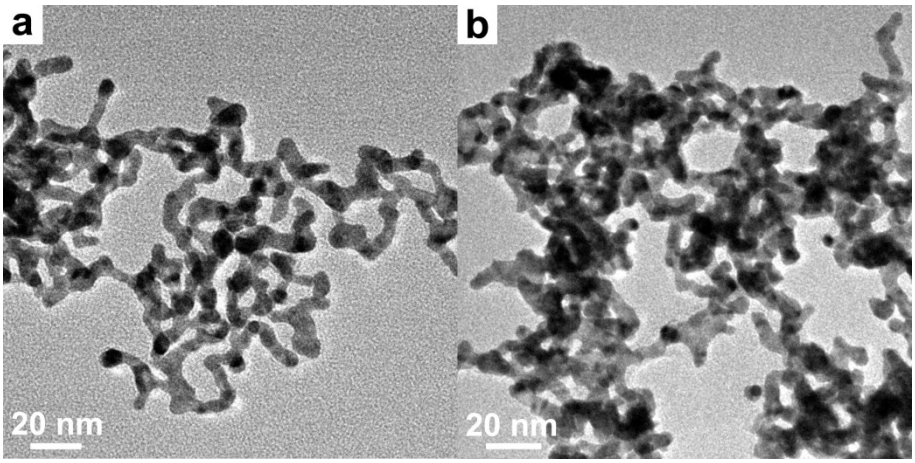

Fig. S26 TEM images of commercial Pt/C catalysts before (a) and after (b) the ADT of 2k cycles.

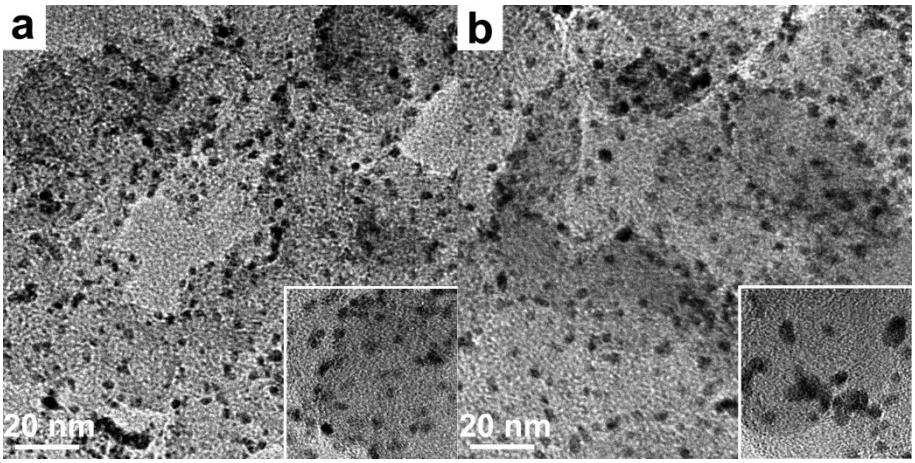

Fig. S27 HAADF–STEM image (a), HAADF–STEM–EDS mapping images (b, c, d, and e) and HAADF–STEM–EDS spectrum (f) of S-doped AuPbPt alloy NWNs after ADT test. The elements in (b), (c), (d), and (e) are Au (red), Pt (green), Pb (cyan), and S (yellow), respectively.

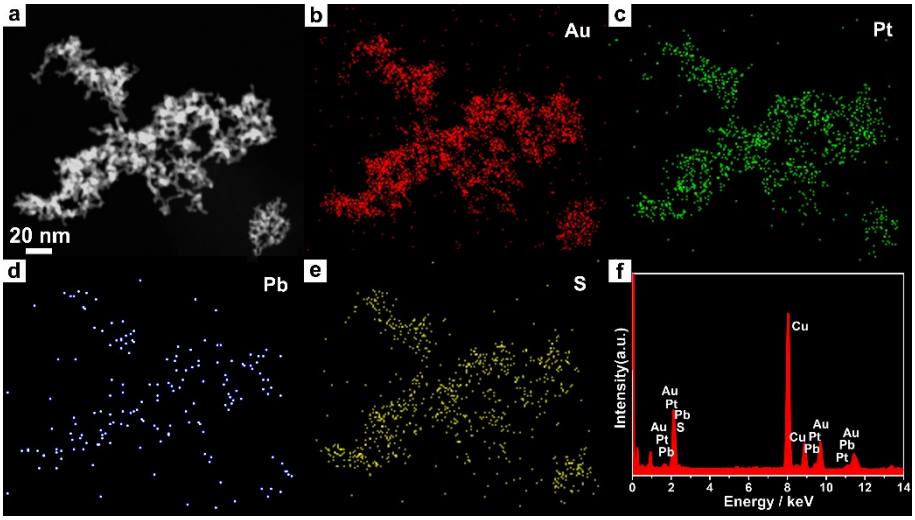

Fig. S28 Chronoamperometric (CA) curves of S-doped AuPbPt alloy NWNs (red curve) and commercial Pt/C catalysts (black curve) at 0.5 V (vs RHE) in O_2-saturated 0.1 M $HClO_4$ at a rotation speed of 1600 rpm.

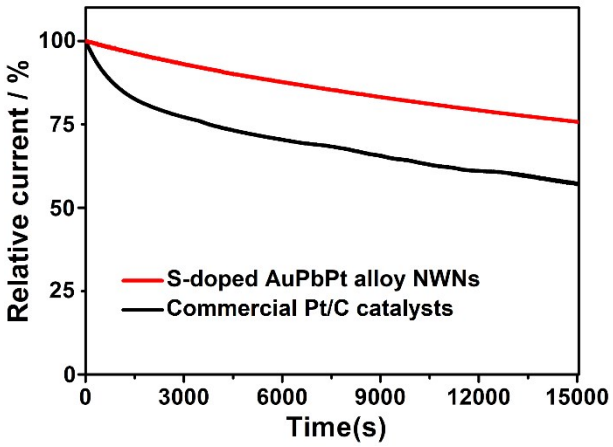

Fig. S29 TOF curves (A) and histograms (B) of TOF value at the overpotential of 0.05 V (vs RHE) of S-doped AuPbPt alloy NWNs (red color) and commercial Pt/C catalysts (black color).

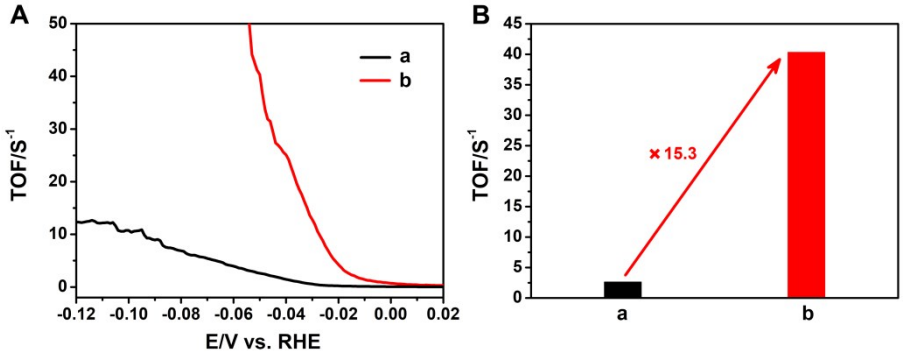

The turnover frequency (TOF) is obtained according to the following equation:[9]

$$TOF = \frac{I}{2Fn}$$

where I is the current, F is the faraday constant (96485 C mol^{-1}), and n is the number of moles of Pt.

Fig. S30 CV curves of S-doped AuPbPt alloy NWNs (red curve) and commercial Pt/C catalysts (black curve) in N_2-saturated 0.5 M H_2SO_4 solution at a scan rate of 50 mV s^{-1}.

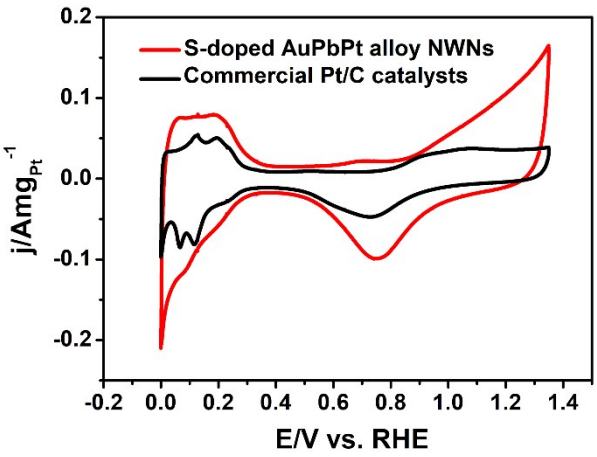

The calculated electrochemically active surface area (ECSA) of S-doped AuPbPt alloy NWNs (143.32 m^2 g^{-1}) is indeed larger than that of commercial Pt/C catalysts (86.29 m^2 g^{-1}), on the basis of CV curves (Fig. S30). The result indicates that S-doped AuPbPt alloy NWNs have more active sites on their surface.

Fig. S31. EIS spectra of S-doped AuPbPt alloy NWNs (red color) and commercial Pt/C catalysts (black color).

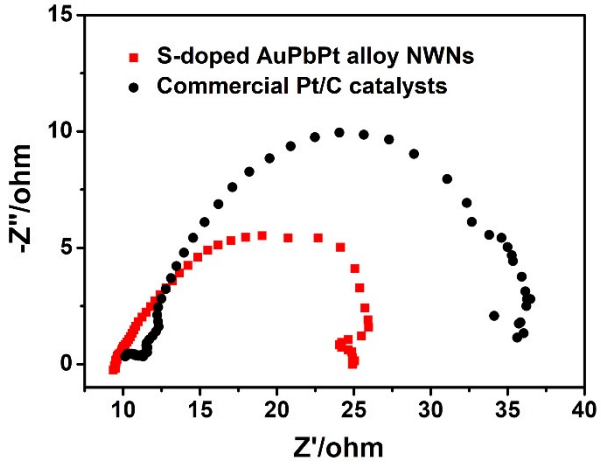

Fig. S32 LSV curves of commercial Pt/C catalysts before (black curve) and after (red curve) the ADT test of 5k cycles in 0.5 M H_2SO_4 solution.

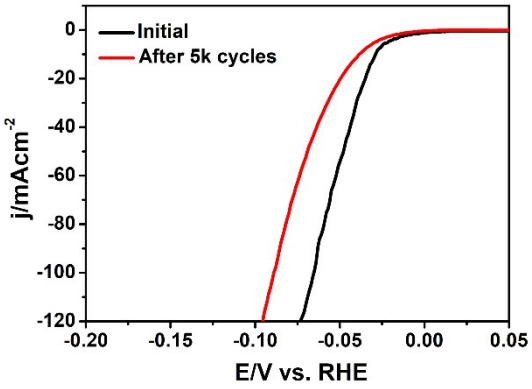

Fig. S33 Tafel plots of S-doped AuPbPt alloy NWNs (A) and commercial Pt/C catalysts (C) before (black curves) and after (red curves) the ADT test of 5k cycles in 0.5 M H_2SO_4 solution, respectively. Histograms of mass activity (at -0.05V vs. RHE) and current density (at -0.07 V vs. RHE) of S-doped AuPbPt alloy NWNs (B) and commercial Pt/C catalysts (D) before (black color) and after (black color) the ADT test of 5k cycles in 0.5 M H_2SO_4 solution, respectively.

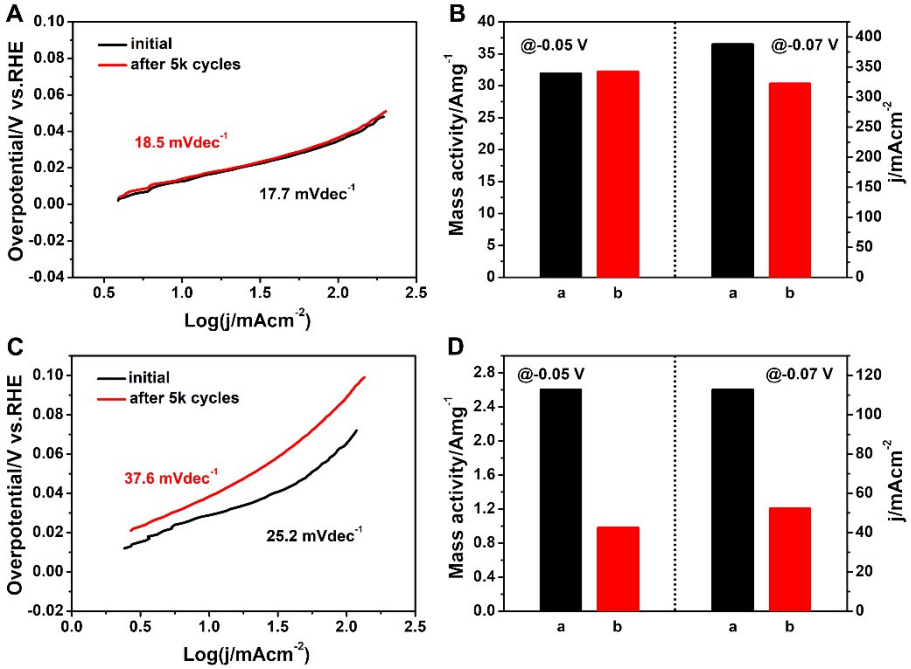

As shown in Fig. S33A, S-doped AuPbPt alloy NWNs show a negligible change in their Tafel plot before and after the ADT test of 5k cycles and their Tafel slopes are also comparable. However, commercial Pt/C catalysts display an obvious change in their Tafel plots and their Tafel slope was increased from 25.2 to 37.6 mV dec^{-1} (Fig. S33C). Moreover, the mass activity (at -0.05 V vs. RHE) of S-doped AuPbPt alloy NWNs was almost unchanged before and after the ADT test of 5k cycles, while that of commercial Pt/C catalysts was only 37.7 % of the initial one (Fig. S33B and D). Furthermore, the current density (at -0.07V vs. RHE) of S-doped AuPbPt alloy NWNs was 83.1 % of the initial one after the ADT test of 5k cycles while that of commercial Pt/C catalysts was 46.3 % of the initial one (Fig. S33B and D). Therefore, the electrocatalytic towards HER of S-doped AuPbPt alloy NWNs is much better than that of commercial Pt/C catalysts.

Fig. S34 TEM image (a), HAADF–STEM image (b), HAADF–STEM–EDS mapping images (c, d and e) and HAADF–STEM–EDS spectrum (f) of the as-prepared AuPbPt NWNs. The elements in (c), (d), and (e) are Au (red), Pt (green), and Pb (cyan), respectively.

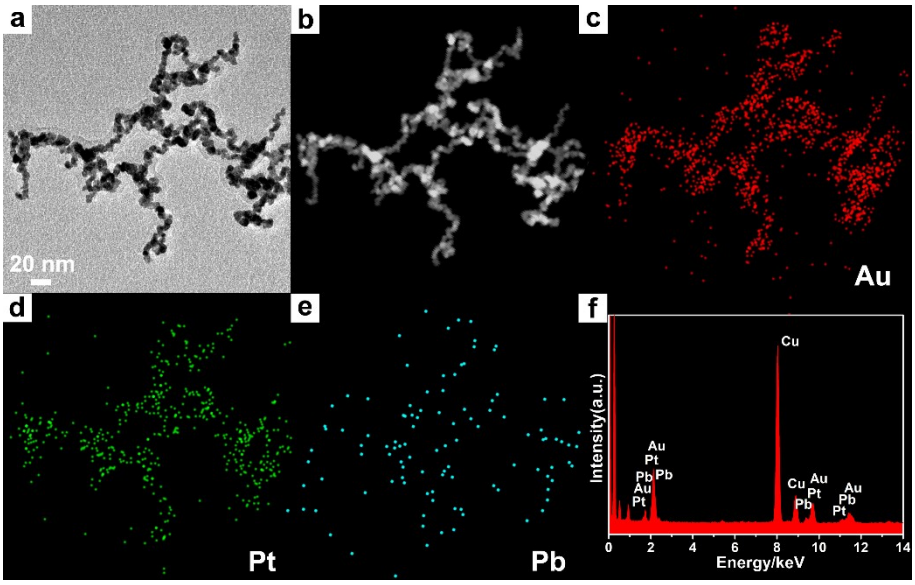

AuPbPt NWNs were synthesized according to our reported method.[10] The detailed synthetic procedure is described as follows. An aqueous solution of $HAuCl_4$ (0.5 mL, 25 mM) were added into the freshly prepared citrate solution (1.0 mL, 34.3 mM). After stirring of 12 min at room temperature, Au NWs with an average diameter of 3nm were formed in the solution, followed by the centrifugation (at 16000 rcf for 4 min) to remove the supernatant and the re-dispersion of them in water. Finally, the AuPbPt NWNs were prepared by using the same procedures used for synthesis of S-doped AuPbPt alloy NWNs except the templates were changed as the as-prepared 3 nm Au NWs.

Fig. S35 LSV curves of the as-prepared S-doped AuPbPt alloy NWNs (a, black curve), commercial Pt/C catalysts (b, red curve), the as-prepared AuPbPt NWNs (c, blue curve) and the as-prepared S-doped AuPb NWNs (d, green curve) in O_2-saturated 0.1 M $HClO_4$ solution at 1600 rpm.

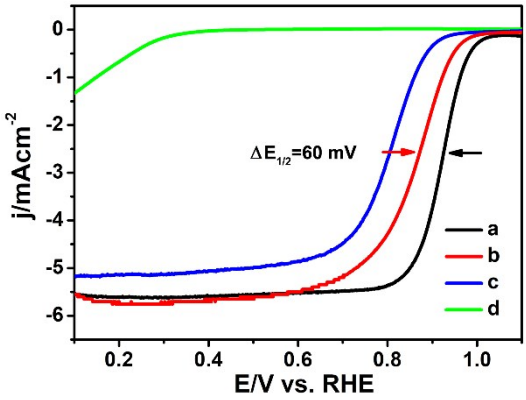

Fig. S36 LSV curves of the as-prepared S-doped AuPbPt alloy NWNs (a, black curve), commercial Pt/C catalysts (b, red curve), the as-prepared AuPbPt NWNs (c, blue curve) and the as-prepared S-doped AuPb NWNs (d, green curve) in N_2-saturated 0.5 M H_2SO_4 solution.

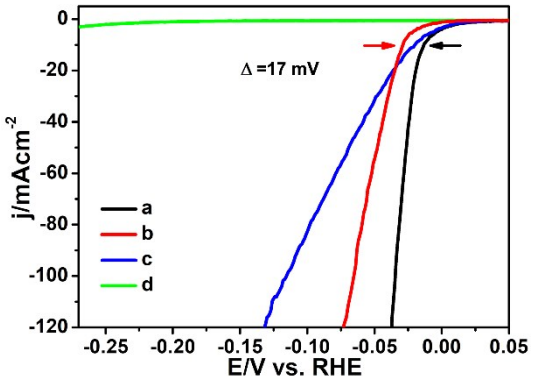

Fig. S37 TEM image (a), HAADF–STEM image (b), HAADF–STEM–EDS mapping images (c and d) and HAADF–STEM–EDS spectrum (e) of the as-prepared PtS nanodendrites. The elements in (c) and (d) are Pt (red) and S (green), respectively.

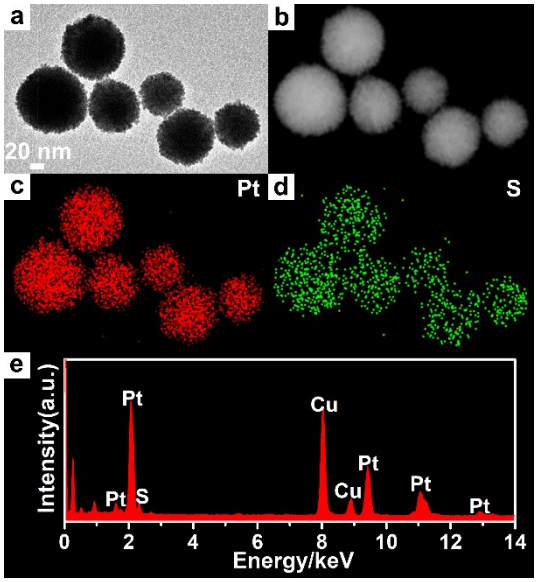

Pt nanodendrites were first synthesized according to our reported method.[11] The detailed synthetic procedure is described as follows. An aqueous solution of K_2PtCl_4 (1.0 mL, 25 mM) were added into the freshly prepared AA solution (1.0 mL, 0.1 M). The mixture solution was sonicated for 30 min. Then, Pt nanodendrites were collected by three repeated rounds of the centrifugation (at 10000 rcf for 10 min) and the washing by Milli-Q water. Next, the Pt nanodendrites were added into the freshly prepared Na_2S solution (2.5 mL, 10 mM) for sufficient sulfidation. Finally, the PtS nanodendrites catalysts were collected by three repeated rounds of the centrifugation (at 10000 rcf for 10 min) and the washing by Milli-Q water.

Fig. S38 TEM image (a), HAADF–STEM image (b), HAADF–STEM–EDS mapping images (c and d) and HAADF–STEM–EDS spectrum (e) of the as-prepared PbS catalysts. The elements in (c) and (d) are Pb (red) and S (green), respectively.

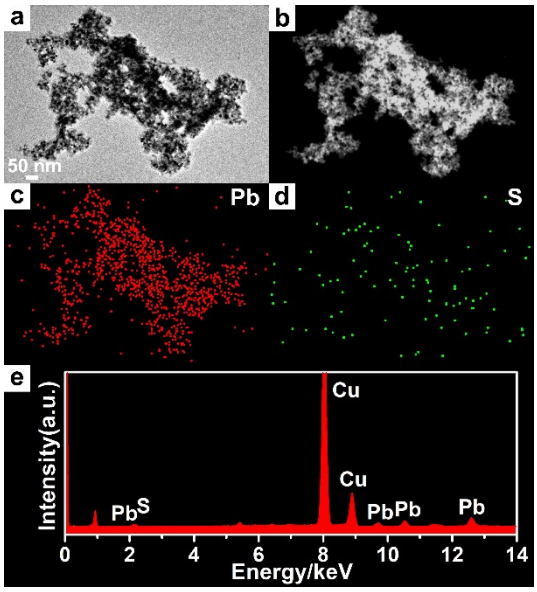

The detailed synthetic procedure for PbS catalysts is described as follows. An aqueous solution of $PbCl_2$ (1.0 mL, 10 mM) was added into the freshly prepared Na_2S solution (2.0 mL, 10 mM) for sufficient sulfidation. Then, the PbS catalysts were collected by three repeated rounds of the centrifugation (at 6000 rcf for 5 min) and the washing by Milli-Q water.

Fig. S39 LSV curves of the as-prepared S-doped AuPbPt alloy NWNs (a, black curve), commercial Pt/C catalysts (b, red curve), PtS nanodendrites (c, blue curve), PbS catalysts (d, green curve) in O_2-saturated 0.1 M $HClO_4$ solution at 1600 rpm.

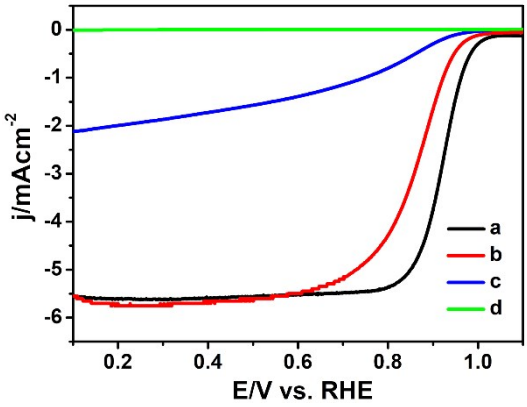

Fig. S40 LSV curves of the as-prepared S-doped AuPbPt alloy NWNs (a, black curve), commercial Pt/C catalysts (b, red curve), PtS nanodendrites (c, blue curve), PbS catalysts (d, green curve) in N_2-saturated 0.5 M H_2SO_4 solution.

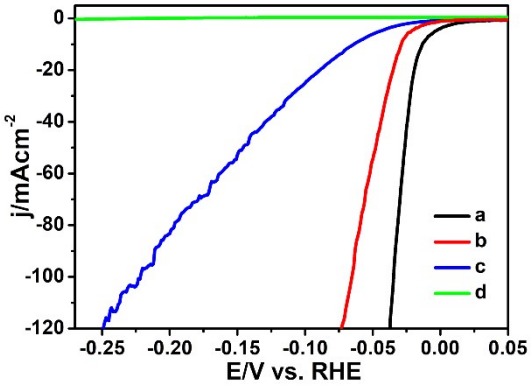

Fig. S41 DFT optimized structures of (A) ORR reaction intermediates (OOH*, O*, OH*) on Pt_4@S-doped Au (111), and Pt_4@ Au (111) surfaces; (B) hydrogen adsorption (H*) on Au (111), Pt (111), Pt_4@S-doped Au (111), and Pt_4@ Au (111) surfaces.

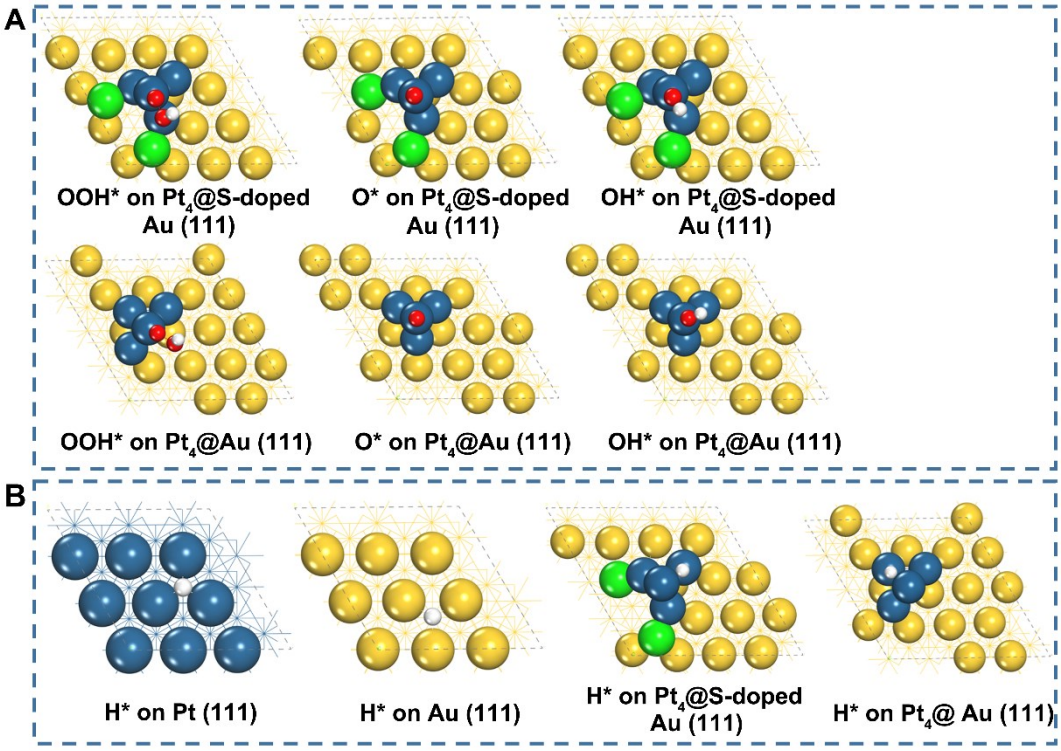

Table S1 Summarized data of the elemental composition of S-doped AuPbPt alloy NWNs determined by ICP-AES.

Sample	Au (%)	Pb (%)	Pt (%)
S-doped AuPbPt alloy NWNs	90.70	1.05	8.25

Table S2 Summarized data of the elemental composition determined by EDS of S-doped AuPb NWNs obtained by the one-time $NaBH_4$ reduction, $NaBH_4$ reduction for two times and $NaBH_4$ reduction for three times. The content of elemental Au in each sample is set as the 100% for better comparison.

Sample	Au (%)	Pb (%)	S (%)
One-time $NaBH_4$ reduction	100	3.86	8.76
$NaBH_4$ reduction for two times	100	1.74	6.47
$NaBH_4$ reduction for three times	100	1.10	2.26

Table S3 Summarized data of electrocatalytic performance towards HER of S-doped $AuPbPt_{0.11}$ alloy NWNs, S-doped $AuPbPt_{0.22}$ alloy NWNs, S-doped $AuPbPt_{0.24}$ alloy NWNs and S-doped $AuPbPt_{0.26}$ alloy NWNs. The subscript number (m) represents the concentration of Pt precursor used for synthesis of S-doped $AuPbPt_m$ alloy NWNs.

Sample	Concentration of Pt precursor [mM]	Overpotential @ 10 mA cm^{-2} [mV]	Tafel slope [mV dec^{-1}]	Mass activity [A mg_{Pt}^{-1}]	j [mA cm^{-2}]
S-doped $AuPbPt_{0.11}$ alloy NWNs	0.11	16	19.5	17.7	181.4
S-doped $AuPbPt_{0.22}$ alloy NWNs	0.22	12	17.7	31.9	387.4
S-doped $AuPbPt_{0.24}$ alloy NWNs	0.24	15	19.4	23.2	317
S-doped $AuPbPt_{0.26}$ alloy NWNs	0.26	14	35.6	9.4	86.5

Table S4 Comparison of ORR performance of S-doped AuPbPt alloy NWNs with other Pt-based electrocatalysts in 0.1 M $HClO_4$ media.

Catalysts	$E_{1/2}$ [V]	Mass Activity [A mg^{-1}]	Reference
S-doped AuPbPt alloy NWNs	0.921	0.59	This work
Pd_cPt_{qms}/C	0.889	-	ACS Catal., 2020, 10, 430-434.[12]
Pt/TOMS	0.90	-	Appl. Catal., B, 2020, 268, 118743.[13]
Pt-NbO_xC	0.918	0.56	Nano Energy, 2020, 69, 104455.[14]
Pt-Au/GNs(1:0.1)	0.85	-	Appl. Surf. Sci., 2020, 508, 145161.[15]
Pt/Ta_2O_5-TaC/C(1000)	0.90	0.297	J. Mater. Chem. A, 2020, 8, 5525-5534.[16]
3ZIF-67-Pt/RGO	0.89	0.208	ACS Appl. Mater. Interfaces, 2020, 12, 9, 10359-10368.[17]
PtNi/GC	~0.91	0.466	ACS Appl. Mater. Interfaces, 2020, 12, 7047-7056.[18]
Pt_6Ru_1/C	0.864	0.287	ACS Sustainable Chem. Eng., 2020, 8, 1295-1301.[19]
PtPd on graphitic nanofibers	-	0.42	Appl. Catal., B, 2019, 259, 118080.[20]
Pt–Ni MNCs	0.91	0.58	J. Mater. Chem. A, 2019, 7, 9791-9797.[21]
Pt@MoS_2/NrGO	0.895	-	ACS Appl. Mater. Interfaces, 2019, 11, 12504-12515.[22]
PtCu NSs/C	0.893	0.42	J. Catal., 2019, 375, 164-170.[23]
$Pt_{0.8}Ni_{0.2}$/C	0.818	0.39	ACS Sustainable Chem. Eng., 2019, 7, 6541-6549.[24]
Pt@NC/C	0.882	0.1165	Langmuir, 2019, 35, 2580-2586.[25]

Table S5 Summarized data of the elemental composition of S-doped AuPbPt alloy NWNs determined by EDS before and after the ADT test.

	Au (%)	Pt (%)	S (%)	Pb (%)
Before ADT test	85.80	11.90	1.50	0.80
After ADT test [a)]	87.53	10.31	1.38	0.78
After ADT test [b)]	85.80	10.11	1.35	0.76
Loss of each element before and after ADT test	0	1.79	0.15	0.04

[a)]The original composition of each element; [b)]The normalized composition of each element.

Given the stability of Au during ADT tests as well as its high content, the content of Au may stay unchanged before and after ADT tests. Therefore, the content of Au in the S-doped AuPbPt alloy NWNs before and after ADT tests is used as the reference to normalize the contents of other elements. As shown in Table S5, the content of Pt, S and Pb in S-doped AuPbPt alloy NWNs after ADT test is reduced from 11.90 to 10.11%, from 1.50 to 1.35%, from 0.80 to 0.76%, respectively. One can clearly see that only about 1.79% of Pt is lost during the ADT process while the loss of S (0.15%) and Pb (0.04%) can be neglected. Taken these results together, the loss of PtS and PbS is about 0.11% and 0.04%, respectively. Therefore, the percentage of Pt loss in ORR is rather low.

Table S6 Comparison of HER performance of S-doped AuPbPt alloy NWNs with other Pt-based electrocatalysts in 0.5 M H_2SO_4 media.

Catalysts	Overpotential @ 10 mA cm^{-2} [mV]	Tafel slope [mV dec^{-1}]	Mass Activity @-0.05 V [A mg_{Pt}^{-1}]	Reference
S-doped AuPbPt alloy NWNs	**12**	**17.7**	**31.9**	**This work**
PtW_6O_{24}/C	22	29.8	20.175@77mV	Nat. Commun., 2020, 11, 490.[26]
Pt/α-MoC_{1-x}-CNFs	38	27	3.49	J. Mater. Chem. A, 2020, 8, 4911-4919.[27]
3ZIF-67-Pt/RGO	14.3	12.5	-	ACS Appl. Mater. Interfaces, 2020, 12, 10359-10368.[17]
H-PtNiCu-AAT NPs	32	33	1.2	ACS Appl. Mater. Interfaces, 2020, 12, 9600-9608.[28]
EG-Pt/CoP-1.5	21	41	-	Energy Environ. Sci., 2019, 12, 2298-2304.[29]
Pt SA/WO_{3-x}	38	45	12.8	Angew. Chem. Int. Ed., 2019, 58, 16038-16042.[30]
PtRu dimers	-	28.9	23.1	Nat. Commun., 2019, 10, 4936.[31]
AL-Pt/Pd_3Pb	13.8	-	7.834	J. Am. Chem. Soc., 2019, 141, 19964-19968.[32]
Pt/f-MWCNTs	43.9	30	18.16	Nano Energy, 2019, 63, 103849.[33]
Pt/$Ti_3C_2T_x$-550	32.7	32.3	1.3	Nano Lett., 2019, 19, 5102-5108.[34]
AC Pt-NG/C	35.28	31	6.508	ACS Catal., 2019, 9, 8213-8223.[35]
Pt/CNTs-ECR	34	26	-	J. Mater. Chem. A, 2019, 7, 15364-15370.[36]
PtNi/10PG CNCs	30.98	18	-	J. Mater. Chem. A, 2019, 7, 17790-17796.[37]
Pt/def-WO_3@CFC	42	61	0.764	J. Mater. Chem. A, 2019, 7, 6285-6293.[38]
MoC_{1-x}/Pt-600-NPs	30	59	-	Adv. Sci., 2019, 6, 1802135.[39]
bβ-Ni_2P_2O·/Pt	28	32	-	ACS Appl. Mater. Interfaces, 2019, 11, 4969-4982.[40]
Mo_2C@NC@P	27	28	-	ACS Appl. Mater. Interfaces, 2019, 11, 4047-4056.[41]

Table S7 Summarized data of EIS results of S-doped AuPbPt alloy NWNs and commercial Pt/C catalysts.

Sample	R_s (Ω)	R_{ct} (Ω)
S-doped AuPbPt alloy NWNs	9.4	15.7
Commercial Pt/C catalysts	10.2	24.3

Table S8 HER performance of S-doped AuPbPt alloy NWNs before and after the ADT test of 5000 cycles.

Sample	Tafel slope [mV dec^{-1}]	Mass activity @-0.05V (vs RHE) [A mg_{Pt}^{-1}]	j @-0.07 V (vs RHE) [mA cm^{-2}]
Before the ADT test	17.7	31.9	387.4
After the ADT test	18.5	32.2	322

Table S9 HER performance of commercial Pt/C catalysts before and after the ADT test of 5000 cycles.

Sample	Tafel slope [mV dec^{-1}]	Mass activity @-0.05 V (vs RHE) [A mg_{Pt}^{-1}]	j@-0.07 V (vs RHE) [mA cm^{-2}]
Before the ADT test	25.2	2.6	112.8
After the ADT test	37.6	0.98	52.2

Table S10 Optimized fractional coordinates for the Pt_4@S-doped Au (111) surface and Pt_4@ Au (111) surface.

Pt_4@S-doped Au (111)

AuPtS-Pt4-doubS

1.00000000000000

11.5352001190000006 0.0000000000000000 0.0000000000000000

-5.7676000595000003 9.9897763408000007 0.0000000000000000

0.0000000000000000 0.0000000000000000 22.0638008118000002

Au S Pt

62 2 4

Selective dynamics

Direct

0.0000000000000000	0.0000000000000000	0.0000000000000000	F	F	F
0.0176247391117541	0.0318049126428641	0.3357700815355553	T	T	T
0.1650913537031009	0.0820180581100644	0.2188348260603271	T	T	T
0.0833299984437517	0.1666700005284270	0.1067200002884690	F	F	F
0.2500000000216716	0.0000000000000000	0.0000000000000000	F	F	F
0.2636015743557850	0.0000505538431905	0.3370447844431169	T	T	T
0.4153926363260759	0.0821186018337656	0.2182996013768992	T	T	T
0.3333300190979216	0.1666700005284270	0.1067200002884690	F	F	F
0.5000000000433431	0.0000000000000000	0.0000000000000000	F	F	F
0.5111712444620005	0.0049480317687459	0.3295251487557743	T	T	T
0.6679414925458624	0.0861561636252782	0.2161442310828676	T	T	T
0.5833299570487185	0.1666700005284270	0.1067200002884690	F	F	F
0.7499999586266384	0.0000000000000000	0.0000000000000000	F	F	F
0.7627969064918863	0.0166483812702889	0.3304849442986869	T	T	T
0.9212970309553657	0.0881402754469154	0.2187108790075963	T	T	T
0.8333299984220801	0.1666700005284270	0.1067200002884690	F	F	F
0.0000000033826311	0.2500000067869408	0.0000000000000000	F	F	F
-0.0003318900871472	0.2660590549074148	0.3271333482114147	T	T	T
0.1693729553832572	0.3358937958151106	0.2193679475297729	T	T	T
0.0833300077824717	0.4166700192275457	0.1067200002884690	F	F	F
0.2500000034043026	0.2500000067869408	0.0000000000000000	F	F	F
0.4102325201092240	0.3263796020798993	0.2141647963860791	T	T	T
0.3333300284366416	0.4166700192275457	0.1067200002884690	F	F	F
0.4999999827067896	0.2500000067869408	0.0000000000000000	F	F	F
0.5036168283661020	0.2507806579169477	0.3290333089773523	T	T	T
0.6672067017144879	0.3362015980856497	0.2189600564493442	T	T	T
0.5833299871066302	0.4166700192275457	0.1067200002884690	F	F	F
0.7499999413767711	0.2500000067869408	0.0000000000000000	F	F	F
0.7502509458493374	0.2601624727352430	0.3307408768504532	T	T	T
0.9178746875718842	0.3375510169428201	0.2156655618494109	T	T	T

0.8333299871283018	0.4166700192275457	0.1067200002884690	F	F	F
0.0000000067652692	0.5000000135738745	0.0000000000000000	F	F	F
-0.0327479184708732	0.5192218488987972	0.3509875174458543	T	T	T
0.1645689690740756	0.5848495948977601	0.2169323586452689	T	T	T
0.0833299905326044	0.6666700260144793	0.1067200002884690	F	F	F
0.2500000067869408	0.5000000135738745	0.0000000000000000	F	F	F
0.4129229341576647	0.5875573598277587	0.2132686517677719	T	T	T
0.3333300111867814	0.6666700260144793	0.1067200002884690	F	F	F
0.5000000068086123	0.5000000135738745	0.0000000000000000	F	F	F
0.6680120983966492	0.5866729188057502	0.2160005040773290	T	T	T
0.5833299698567629	0.6666700260144793	0.1067200002884690	F	F	F
0.7499999654785938	0.5000000135738745	0.0000000000000000	F	F	F
0.7352564313859901	0.5157698963123633	0.3403645494539376	T	T	T
0.9157570402909033	0.5849705903566782	0.2210298490007174	T	T	T
0.8333299697917411	0.6666700260144793	0.1067200002884690	F	F	F
0.0000000308170343	0.7500000202607140	0.0000000000000000	F	F	F
0.0063013478342513	0.7711915343541682	0.3315996680518716	T	T	T
0.1669347308553043	0.8344355868463665	0.2205865035456863	T	T	T
0.0833300351802393	0.9166700328014201	0.1067200002884690	F	F	F
0.2500000308387129	0.7500000202607140	0.0000000000000000	F	F	F
0.2618435781584788	0.7526055658994443	0.3308390860352824	T	T	T
0.4183424510135775	0.8347319749812673	0.2181960134090641	T	T	T
0.3333300352019108	0.9166700328014201	0.1067200002884690	F	F	F
0.5000000307736912	0.7500000202607140	0.0000000000000000	F	F	F
0.5194794191768045	0.7682180758788836	0.3421687304015751	T	T	T
0.6665099530343001	0.8354632532732380	0.2203777559327757	T	T	T
0.5833299938718923	0.9166700328014201	0.1067200002884690	F	F	F
0.7499999894436797	0.7500000202607140	0.0000000000000000	F	F	F
0.7667093499103595	0.7745391896054205	0.3405744486390648	T	T	T
0.9151144146575532	0.8372639145689910	0.2196934377105401	T	T	T
0.8333299938935639	0.9166700328014201	0.1067200002884690	F	F	F
0.4803607563629813	0.4929255910441787	0.3107706952342228	T	T	T
0.2024434788369995	0.1146242204259408	0.4093876920954284	T	T	T
0.1631389429999923	0.5008380785845038	0.3524773419458958	T	T	T
0.3436038624292781	0.5438705068832050	0.4028647718889010	T	T	T
0.4134070324863854	0.4740738118510076	0.5016700542133510	T	T	T
0.3740006158530279	0.3208872017297728	0.4096359553351117	T	T	T
0.5913691155753914	0.5856627258365128	0.4201056445224388	T	T	T

Pt_4@ Au (111)

Pt4-Au111

1.00000000000000

11.7488002776999991 0.0000000000000000 0.0000000000000000

-5.8744001388999996 10.1747595045000008 0.0000000000000000

0.0000000000000000 0.0000000000000000 22.1947002411000014

Au Pt

64 4

Selective dynamics

Direct

0.0000000000000000	0.0000000000000000	0.0000000000000000	F	F	F
-0.0036467114366916	-0.0081172640063804	0.3274853455498919	T	T	T
0.1643286661847190	0.0773521242135573	0.2151060736339676	T	T	T
0.0833300008628939	0.1666699961065419	0.1080499986460381	F	F	F
0.2499999999638263	0.0000000000000000	0.0000000000000000	F	F	F
0.2468554691960346	-0.0090643140501586	0.3267390487906506	T	T	T
0.4150931155835696	0.0794046722329985	0.2141314555452202	T	T	T
0.3333300059336253	0.1666699961065419	0.1080499986460381	F	F	F
0.5000000000127685	0.0000000000000000	0.0000000000000000	F	F	F
0.5007127388874031	0.0021992008352517	0.3254172476026836	T	T	T
0.6680323107642578	0.0819897083938149	0.2148767084366535	T	T	T
0.5833299653826742	0.1666699961065419	0.1080499986460381	F	F	F
0.7499999593767015	0.0000000000000000	0.0000000000000000	F	F	F
0.7549534610066209	0.0036109829058537	0.3256962298626398	T	T	T
0.9166714552332410	0.0820315365693451	0.2162483886514785	T	T	T
0.8333300059463937	0.1666699961065419	0.1080499986460381	F	F	F
0.0000000043931578	0.2500000088331333	0.0000000000000000	F	F	F
-0.0034765707521779	0.2426746090387889	0.3374267644535061	T	T	T
0.1636235197220398	0.3248471910424140	0.2127167383484770	T	T	T
0.0833300162107662	0.4166700166352797	0.1080499986460381	F	F	F
0.2500000044421000	0.2500000088331333	0.0000000000000000	F	F	F
0.2418216407400479	0.2274633213201559	0.3271715998007104	T	T	T
0.4141423224812146	0.3278112040693806	0.2151003548079735	T	T	T
0.3333300162597013	0.4166700166352797	0.1080499986460381	F	F	F
0.4999999841485376	0.2500000088331333	0.0000000000000000	F	F	F
0.4995372177962775	0.2376187645540256	0.3247952220620225	T	T	T
0.6670905382517716	0.3312791363813080	0.2148257416802293	T	T	T
0.5833299959661460	0.4166700166352797	0.1080499986460381	F	F	F
0.7499999435124778	0.2500000088331333	0.0000000000000000	F	F	F
0.7503493269531953	0.2464873053640735	0.3265201091475969	T	T	T
0.9186376409837679	0.3313320276808319	0.2170071346624167	T	T	T
0.8333299959299723	0.4166700166352797	0.1080499986460381	F	F	F
0.0000000088714316	0.5000000176662667	0.0000000000000000	F	F	F

-0.0100345852224199	0.4955870648462005	0.3280120248903264	T	T	T
0.1627240276334173	0.5877631262845820	0.2111906809552657	T	T	T
0.0833300120912881	0.6666700489579114	0.1080499986460381	F	F	F
0.2500000088352579	0.5000000176662667	0.0000000000000000	F	F	F
0.2322420377248370	0.4944923111798087	0.3078662310298583	T	T	T
0.4191655117966049	0.5830697194479340	0.2143690612963151	T	T	T
0.3333300121402232	0.6666700489579114	0.1080499986460381	F	F	F
0.5000000087990841	0.5000000176662667	0.0000000000000000	F	F	F
0.4911600786018447	0.4720331351283455	0.3234401147460472	T	T	T
0.6644751027242072	0.5805100367949092	0.2160796251419403	T	T	T
0.5833299918466679	0.6666700489579114	0.1080499986460381	F	F	F
0.7499999682481402	0.5000000176662667	0.0000000000000000	F	F	F
0.7465595982666728	0.4935389476733187	0.3273204549457936	T	T	T
0.9122319087262620	0.5792356556757858	0.2155058152065676	T	T	T
0.8333299918104871	0.6666700489579114	0.1080499986460381	F	F	F
0.0000000452667308	0.7500000499888984	0.0000000000000000	F	F	F
-0.0037101864714497	0.7444915851120979	0.3273012629742575	T	T	T
0.1632917528224087	0.8318943459559173	0.2162975493671629	T	T	T
0.0833300281800504	0.9166700811822608	0.1080499986460381	F	F	F
0.2500000453156730	0.7500000499888984	0.0000000000000000	F	F	F
0.2429679152382185	0.7493088005434371	0.3311454703857266	T	T	T
0.4150763046570484	0.8326842537769296	0.2149826233019379	T	T	T
0.3333300078864880	0.9166700811822608	0.1080499986460381	F	F	F
0.5000000452794993	0.7500000499888984	0.0000000000000000	F	F	F
0.5073397215552495	0.7666845267364627	0.3202747557144648	T	T	T
0.6697583474405214	0.8326215919969983	0.2153432426783504	T	T	T
0.5833299875929328	0.9166700811822608	0.1080499986460381	F	F	F
0.7500000047285482	0.7500000499888984	0.0000000000000000	F	F	F
0.7539482935572570	0.7482331753086212	0.3301404745285698	T	T	T
0.9143292336761172	0.8292628040884372	0.2162195952251124	T	T	T
0.8333299876418678	0.9166700811822608	0.1080499986460381	F	F	F
0.3273488309662294	0.6339577829052432	0.4111430529040453	T	T	T
0.2114051713009724	0.3722278419035571	0.4112292644567623	T	T	T
0.5586150180829487	0.6449215065143248	0.4110837457841264	T	T	T
0.3844656782316896	0.5102756928147609	0.4898000071939031	T	T	T

Computational Methods

Periodic density functional theory (DFT) calculations were performed with the Perdew–Burke–Ernzerhof (PBE) exchange–correlation functional[42] and the projector-augmented wave (PAW) method.[43-44] All DFT calculations were performed using Vienna Ab initio Simulation Package (VASP).[45-48] The recommended default potentials were employed for all elements (Pt, S, Au, O, and H), and an energy cutoff of 400 eV was used throughout this work. Spin polarization was also applied in all the calculations. The electronic energy of the supercell was converged to 10^{-6} eV in the self-consistent field calculations, whereas the force on each relaxed atom was converged to 0.02 eV $Å^{-1}$ in the ionic relaxation calculations.

For the S-doped AuPbPt alloy nanowire-network (NWNs) catalyst, our experimental results show that the catalyst was mainly composed of Au, Pt, S, and Pb, with the ratio of 85.8, 11.9, 1.5, and 0.8%, respectively. Due to the low concentration of Pb, the Pb element was not considered in our simulations. In the proposed structure model of the S-doped AuPbPt NWNs catalyst, the p(4×4) Au (111) supercell was used as the substrate, and the surface was doped with two S atoms. A tetrahedral Pt_4 cluster with the T_d symmetry[49,50] was then constructed and anchored on the S-doped Au (111) surface. The bottom two layers of the four-layer Au (111) slab model were fixed at their bulk positions. A vacuum layer of 15 Å was inserted between adjacent slabs, and Gamma centered k-point mesh of (2×2×1) was applied.

To calculate the free energy diagram of the ORR, the computational hydrogen electrode (CHE) model was used. The ORR reaction involves four electron-proton transfer steps,[51-55] and the detailed reaction pathway is shown as:

$$* + O_2 + H^+ + e^- \rightarrow OOH* \quad (1)$$

$$OOH* + H^+ + e^- \rightarrow O* + H_2O \quad (2)$$

$$O* + H^+ + e^- \rightarrow OH* \quad (3)$$

$$OH* + H^+ + e^- \rightarrow H_2O \quad (4)$$

where * denotes the active site on the surface of the catalyst. The Gibbs free energies for the four elementary steps mentioned above are related to the Gibbs free energies of the various intermediate species. The free energy of these intermediate species are calculated using the expression: $G = E_{elect} + ZPE - T*S$, where the E_{elect} is the electronic energy from the DFT calculations, ZPE and T*S are the zero-point energy and the entropy of the adsorbed species, which was calculated from the vibrational frequencies. T is the temperature (298.15 K in this work). Entropies of the gaseous species (H_2O, H_2, and O_2) are calculated from available experimental values.[56,57]

References

1. G. Shi, H. Yano, D. A. Tryk, A. Iiyama and H. Uchida, *ACS Catal.*, 2016, **7**, 267-274.
2. L. Gao, X. Li, Z. Yao, H. Bai, Y. Lu, C. Ma, S. Lu, Z. Peng, J. Yang, A. Pan and H. Huang, *J. Am. Chem. Soc.*, 2019, **141**, 18083-18090.
3. P. Song, S.-S. Li, L.-L. He, J.-J. Feng, L. Wu, S.-X. Zhong and A.-J. Wang, *RSC Adv.*, 2015, **5**, 87061-87068.
4. C. Wu, H. Li, H. He, Y. Song, C. Bi, W. Du and H. Xia, *ACS Appl. Mater. Interfaces*, 2019, **11**, 46902-46911.
5. L. Wang, X. Wu, S. Guo, M. Han, Y. Zhou, Y. Sun, H. Huang, Y. Liu and Z. Kang, *J. Mater. Chem. A*, 2017, **5**, 2717-2723.
6. M. A. Peck and M. A. Langell, *Chem. Mater.*, 2012, **24**, 4483-4490.
7. Y. Kim, J. W. Hong, Y. W. Lee, M. Kim, D. Kim, W. S. Yun and S. W. Han, *Angew. Chem., Int. Ed.*, 2010, **49**, 10197-10201.
8. P. K. Sonkar, K. Prakash, M. Yadav, V. Ganesan, M. Sankar, R. Gupta and D. K. Yadav, *J. Mater. Chem. A*, 2017, **5**, 6263-6276.
9. X.-K. Wan, H. B. Wu, B. Y. Guan, D. Luan and X. W. Lou, *Adv. Mater.*, 2020, **32**, 1901349.
10. J. Wang, P. Zhang, Y. Xiahou, D. Wang, H. Xia and H. Mohwald, *ACS Appl. Mater. Interfaces*, 2018, **10**, 602-613.
11. Y. Li, W. Ding, M. Li, H. Xia, D. Wang and X. Tao, *J. Mater. Chem. A*, 2015, **3**, 368-376.
12. X. Wang, Y. Orikasa, M. Inaba and Y. Uchimototo, *ACS Catal.*, 2020, **10**, 430-434.
13. R. A. M. Esfahani and E. B. Easton, *Appl.Catal., B*, 2020, **268**, 118743.
14. Z. Ma, S. Li, L. Wu, L. Song, G. Jiang, Z. Liang, D. Su, Y. Zhu, R. R. Adzic, J. X. Wang and Z. Chen, *Nano Energy*, 2020, **69**, 104455.
15. Y. Xie, Z. Li, Y. Liu, Y. Ye, X. Zou and S. Lin, *Appl. Surf. Sci.*, 2020, **508**, 145161.
16. W. Gao, T. Liu, Z. Zhang, M. Dou and F. Wang, *J. Mater. Chem. A*, 2020, **8**, 5525-5534.
17. W. Wu, Z. Zhang, Z. Lei, X. Wang, Y. Tan, N. Cheng and X. Sun, *ACS Appl. Mater. Interfaces*, 2020, **12**, 10359-10368.
18. J. Wang, Q. Xue, B. Li, D. Yang, H. Lv, Q. Xiao, P. Ming, X. Wei and C. Zhang, *ACS Appl. Mater. Interfaces*, 2020, **12**, 7047-7056.
19. Y. Liu, L. Du, F. Kong, G. Han, Y. Gao, C. Du, P. Zuo and G. Yin, *ACS Sustainable Chem. Eng.*, 2019, **8**, 1295-1301.
20. Y.-X. Xiao, J. Ying, G. Tian, Y. Tao, H. Wei, S.-Y. Fan, Z.-H. Sun, W.-J. Zou, J. Hu, G.-G. Chang, W. Li, X.-Y. Yang and C. Janiak, *Appl.Catal., B*, 2019, **259**, 118080.
21. K. Deng, Y. Xu, D. Yang, X. Qian, Z. Dai, Z. Wang, X. Li, L. Wang and H. Wang, *J. Mater. Chem. A*, 2019, **7**, 9791-9797.
22. S. Ramakrishnan, M. Karuppannan, M. Vinothkannan, K. Ramachandran, O. J. Kwon and D. J. Yoo, *ACS Appl. Mater. Interfaces*, 2019, **11**, 12504-12515.

23. W. Li, Z.-Y. Hu, Z. Zhang, P. Wei, J. Zhang, Z. Pu, J. Zhu, D. He, S. Mu and G. Van Tendeloo, *J. Catal.*, 2019, **375**, 164-170.
24. J. Liu, J. Lan, L. Yang, F. Wang and J. Yin, *ACS Sustainable Chem. Eng.*, 2019, **7**, 6541-6549.
25. J. Liu, W. Li, R. Cheng, Q. Wu, J. Zhao, D. He and S. Mu, *Langmuir*, 2019, **35**, 2580-2586.
26. F.-Y. Yu, Z.-L. Lang, L.-Y. Yin, K. Feng, Y.-J. Xia, H.-Q. Tan, H.-T. Zhu, J. Zhong, Z.-H. Kang and Y.-G. Li, *Nat. Commun.*, 2020, **11**, 490.
27. X. Pan, S. Lu, D. Zhang, Y. Zhang, F. Duan, H. Zhu, H. Gu, S. Wang and M. Du, *J. Mater. Chem. A*, 2020, **8**, 4911-4919.
28. D. Wu, W. Zhang, A. Lin and D. Cheng, *ACS Appl. Mater. Interfaces*, 2020, **12**, 9600-9608.
29. J. Li, H.-X. Liu, W. Gou, M. Zhang, Z. Xia, S. Zhang, C.-R. Chang, Y. Ma and Y. Qu, *Energy Environ. Sci.*, 2019, **12**, 2298-2304.
30. J. Park, S. Lee, H. E. Kim, A. Cho, S. Kim, Y. Ye, J. W. Han, H. Lee, J. H. Jang and J. Lee, *Angew. Chem., Int. Ed.*, 2019, **58**, 16038-16042.
31. L. Zhang, R. Si, H. Liu, N. Chen, Q. Wang, K. Adair, Z. Wang, J. Chen, Z. Song, J. Li, M. N. Banis, R. Li, T.-K. Sham, M. Gu, L.-M. Liu, G. A. Botton and X. Sun, *Nat. Commun.*, 2019, **10**, 4936.
32. Y. Yao, X.-K. Gu, D. He, Z. Li, W. Liu, Q. Xu, T. Yao, Y. Lin, H.-J. Wang, C. Zhao, X. Wang, P. Yin, H. Li, X. Hong, S. Wei, W.-X. Li, Y. Li and Y. Wu, *J. Am. Chem. Soc.*, 2019, **141**, 19964-19968.
33. J. Ji, Y. Zhang, L. Tang, C. Liu, X. Gao, M. Sun, J. Zheng, M. Ling, C. Liang and Z. Lin, *Nano Energy*, 2019, **63**, 103849.
34. Z. Li, Z. Qi, S. Wang, T. Ma, L. Zhou, Z. Wu, X. Luan, F.-Y. Lin, M. Chen, J. T. Miller, H. Xin, W. Huang and Y. Wu, *Nano Lett.*, 2019, **19**, 5102-5108.
35. M. Sun, J. Ji, M. Hu, M. Weng, Y. Zhang, H. Yu, J. Tang, J. Zheng, Z. Jiang, F. Pan, C. Liang and Z. Lin, *ACS Catal.*, 2019, **9**, 8213-8223.
36. X. Bao, Y. Gong, Y. Chen, H. Zhang, Z. Wang, S. Mao, L. Xie, Z. Jiang and Y. Wang, *J. Mater. Chem. A*, 2019, **7**, 15364-15370.
37. J. Yang, G. Ning, L. Yu, Y. Wang, C. Luan, A. Fan, X. Zhang, Y. Liu, Y. Dong and X. Dai, *J. Mater. Chem. A*, 2019, **7**, 17790-17796.
38. H. Tian, X. Cui, L. Zeng, L. Su, Y. Song and J. Shi, *J. Mater. Chem. A*, 2019, **7**, 6285-6293.
39. H. J. Song, M. C. Sung, H. Yoon, B. Ju and D. W. Kim, *Adv. Sci.*, 2019, **6**, 1802135.
40. J. Theerthagiri, E. S. F. Cardoso, G. V. Fortunato, G. A. Casagrande, B. Senthilkumar, J. Madhavan and G. Maia, *ACS Appl. Mater. Interfaces*, 2019, **11**, 4969-4982.
41. J. Q. Chi, J. Y. Xie, W. W. Zhang, B. Dong, J. F. Qin, X. Y. Zhang, J. H. Lin, Y. M. Chai and C. G. Liu, *ACS Appl. Mater. Interfaces*, 2019, **11**, 4047-4056.
42. J. P. Perdew, K. Burke and M. Ernzerhof, *Phys. Rev. Lett*., 1996, **77**, 3865.
43. P. E. Blöchl, *Phys. Rev. B: Condens. Matter Mater. Phys*., 1994, **50**, 17953.
44. G. Kresse and J. Joubert, *Phys. Rev. B: Condens. Matter Mater. Phys.*, 1999,

59, 1758.
45. G. Kresse, J. Hafner. *Phys. Rev. B: Condens. Matter Mater. Phys*. 1993, **47**, 558-561.
46. G. Kresse, J. Hafner. *Phys. Rev. B: Condens. Matter Mater. Phys.* 1994, **49**, 14251-14269.
47. G. Kresse, J. Furthmüller, *Comput. Mater. Sci*. 1996, **6**, 15-50.
48. G. Kresse,; J. Furthmüller. *Phys. Rev. B: Condens. Matter Mater. Phys*. 1996, **54**, 11169-11186.
49. H. K. Yuan, A. L. Kuang, C. L. Tian, and H. Chen. *AIP Advances*. 2014, **4**, 037107.
50. P.Munieswaran, S. Seenithurai, R. Kodi Pandyan, S. Vinodh Kumar, C .Saranya, M. Mahendran. *AIP Conf. Proc.* 2015, **1665**, 050134-1–050134-3.
51. J. Greeley, I. E. L. Stephens, A. S. Bondarenko, T. P. Johansson, H. A. Hansen, T. F. Jaramillo, J. Rossmeisl, I. Chorkendorff, J. K. Nørskov. *Nat. Chem*. 2009, **1**, 552-556.
52. A. Holewinski, J. C. Idrobo, S. Linic. *Nat. Chem.* 2014, **6**, 828-834.
53. Y. Jiao, Y. Zheng, M. Jaroniec, S. Z. Qiao. *J. Am. Chem. Soc*. 2014, **136**, 4394-4403.
54. V. Tripkovic, T. Vegge, *J. Phys. Chem. C* 2017, **121**, 26785-26793.
55. M. Reda, H. A. Hansen, and T. Vegge. *ACS Catal.* 2018, **8**, 10521-10529.
56. W. Haynes, Ed. CRC handbook of chemistry and physics: A ready-reference book of chemical and physical data, 95th ed.; CRC Press: Boca Raton, 2014.
57. National Institute of Standards and Technology (NIST). Computational Chemistry Comparison and Benchmark Database, NIST Standard Reference Database Number 101; NIST: Gaithersburg, MD, 2014. See the following: https://cccbdb.nist.gov/.